**Title:**

Sustained spinal motor activity triggered by direct mechanosensory stimulation in adult *Drosophila melanogaster*

Alexandra M. Medeiros[1], Anna F. Hobbiss[1,2], Gonçalo Borges[1], Marta Moita[2], César S. Mendes[1, 3]

1. iNOVA4Health, NOVA Medical School|Faculdade de Ciências Médicas, NMS|FCM, Universidade Nova de Lisboa; Lisbon, Portugal

2. Champalimaud Research, Champalimaud Center for the Unknown, Lisbon, Portugal

3. Lead contact

Correspondence: cesar.mendes@nms.unl.pt

**Abstract**

Most vertebrates and invertebrates such as *Drosophila melanogaster* are able to move in complex environments due to their ability to integrate sensory information along with motor commands. Mechanosensory structures exist along each leg to assist in motor coordination by transmitting external cues or proprioceptive information to motor centers in the central nervous system.

Nevertheless, how different mechanosensory structures engage these locomotor centers and their underlying circuits remains poorly understood. Here, we tested the role of mechanosensory structures in movement initiation by optogenetically stimulating specific classes of leg sensory structures. We found that stimulation of leg Mechanosensory Bristles (MsB) and femoral Chordotonal Organ (ChO) is sufficient to initiate forward movement in immobile animals. We also found that while the stimulation of the ChO depends on the presence of the central brain to trigger forward movement, stimulation of leg MsB could trigger cyclic motor activity independently of central brain circuits. Leg MsB-triggered movement lacks inter-leg and intra-leg coordination, whilst antagonistic muscle activity within joints is preserved. Moreover, we found that the duration of the MsB-induced movement is dependent on the number of excited cells and is specific to leg afferents, since stimulation of MsB in other segments lead to different motor outcomes. This study sheds light on the ability of specific sensory circuits to modulate motor control, including initiation of movement, and how this information can be automatically translated to a motor command by spinal neuronal pathways.

## Introduction

A remarkable feature of moving organisms is their ability to adapt to external environmental conditions, optimizing speed, stability and energy consumption (Alexander, 2003; Dickinson et al., 2000; Hoyt and Taylor, 1981). Key for this flexibility is mechanosensory feedback, including proprioception and exteroception, enabled by specialized neurons that relay internal and external physical features such as muscle extension, tissue compression or gravitational orientation to motor centers. Lack of sensory feedback renders animals highly uncoordinated, largely determined by the number and class of inactivated cells (Akay et al., 2014; Mendes et al., 2013). Sensory structures vary in shape and properties depending on the type of mechanical feature being transduced (Smith and Shepherd, 1996). For example, in insects, the Chordotonal organ (ChO) relays the mechanical features of joint angles, a structure analogous to mammalian muscle spindles (Tuthill and Wilson, 2016b), whereas Campaniform Sensilla (CS), dome-like structures in the cuticle of the fly leg, sense deformation caused by load (Akay et al., 2001; Tuthill and Wilson, 2016b).

While dendrites of proprioceptors are located in the leg segment containing the sensory cell, axons project into the central nervous system, mostly into the ventral-most layer of the leg neuropil within the Ventral Nerve Chord (VNC), the insect equivalent of the mammalian spinal cord, where sensory information is processed (Court et al., 2020; Merritt and Murphey, 1992; Murphey et al., 1989; Tsubouchi et al., 2017; Tuthill and Wilson, 2016a). Sensory structures interact with local circuits in the VNC in order to modulate and adjust locomotor patterns. However, to generate fully functional and coordinated locomotion, communication between motor circuits and higher order centers is required (Ritzmann and Buschges, 2007). Evidence shows that locally these structures can directly trigger muscle contraction to correct movement and posture. For instance, ChO receptors that sense the position of the femur-tibia joint react to an imposed extension of the tibia by inducing excitation of flexor tibiae motor neurons and at the same time activate local interneurons that inhibit the antagonistic extensor tibiae motor neurons (Burrows et al., 1988). Another example of local modulation by sensory inputs comes from the stick insect, where it was shown that sensory feedback, notably from the

ChO and CS, assists in phase transition from stance to swing phase, a process termed "active reaction", which influences the activation threshold by flexion and extensor motor pools providing a positive reinforcement of movement (Akay and Büschges, 2006; Bassler and Buschges, 1998). Further studies suggest the existence of a local neuronal architecture within the VNC linking particular sensory structures to Central Pattern Generators (CPGs) and leg motor neurons to produce inter-segmental coordination (Borgmann et al., 2011; Tuthill and Wilson, 2016b). These features allow the generation of a continuous, stable and coordinated walking pattern. In addition, this model depicts the role of sensory information not just as correcting or inducing movement via supra spinal motor centers, but also suggests that sensory input can directly engage local circuits triggering or sustaining step cycling.

Another crucial mechanosensory structure are the Mechanosensory Bristles (MsB). These structures are involved in detecting external cues, including dust particles, parasites and wind intensity, triggering varied motor outcomes such as grooming, defensive kicking or locomotion arrest (Li et al., 2016; Mamiya et al., 2018; Seeds et al., 2014; Tsubouchi et al., 2017). In the context of collective behavior, mechanosensory bristles play a role in conspecific avoidance by initiating walking responses triggered by another fly's touch (Ramdya et al., 2015). An avoidance response was also seen after the optogenetic stimulation of mechanosensory bristles in specific legs during walking (DeAngelis et al., 2020). Given that self-generated movement also results in bristle deflection, these structures may also play a role in proprioception, as well as exteroception (Tuthill and Wilson, 2016a).

However, despite their ethological importance, the downstream circuits that integrate information from mechanosensory bristles, and transform it into the appropriate motor response, are unknown. Towards this end, we aimed to understand mechanosensory integration within downstream motor circuits by asking if a particular class of leg sensory neurons, the Mechanosensory Bristles (MsB), could elicit movement, and characterizing the response in comparison with the ChO. For this we took advantage of the rich *Drosophila* genetic tool-kit and kinematic quantitative tools, to address these questions with cellular resolution and detail.

Here we show that stimulation of MsB or ChO is sufficient to initiate forward movement in an immobile fly. Moreover, we found that while leg ChO stimulation depends on the presence of a central brain for flies to engage in forward movement, leg MsB stimulation could trigger sustained motor activity independently of central brain activity. Leg MsB-triggered forward movement lacks inter and intra-leg coordination although antagonistic muscle activity is nevertheless preserved. Moreover, we found that the MsB-evoked response can be triggered from different leg segments and its intensity depends on the number of stimulated bristles. This response is also specific to leg MsB since stimulation in the wing or head lead to different motor outcomes.

This study sheds light on the ability of specific sensory circuits to modulate motor control, including initiation of movement, and how this information can automatically be translated to spinal motor programs. Moreover, it suggests how and what parameters the central brain can control during forward coordinated locomotion.

## Results

### Activation of leg mechanosensory bristles evokes central brain independent movement

To understand the role of leg sensory afferents in movement control and initiation we identified fly lines that targeted the different types of mechanosensory neurons present in the leg. For that, we performed an expression screen for GAL4 lines from the Janelia Flylight Collection that labelled specific sensory structures in the fly leg (Jenett et al., 2012; Pfeiffer et al., 2010). In order to restrict GAL4 expression to the legs, we used a combinatorial approach with flipase under the control of the $Dac^{RE}$ enhancer fragment (Mendes et al., 2013). Among the relevant lines and based on the expression pattern we selected 2 lines, one labelling Mechanosensory Bristles (hereafter termed MsB1) and one labelling the femoral Chordotonal Organ (termed ChO1) (Fig. 1A, B, and S1). Although normally classified as exteroceptors, MsB can additionally be described as proprioceptors since these afferents can also be activated during self-movement, which is supported by the observation that their inactivation causes perturbations in walking patterns (Tuthill and Wilson, 2016a) (Medeiros and Mendes, unpublished). Moreover, we chose ChO lines due to the large body of work focusing on this structure (Agrawal et al., 2020; Chen et al., 2021; Cheng et al., 2010; Jarman et al., 1993; Mamiya et al., 2018; Mendes et al., 2014; Shanbhag et al., 1992; Smith and Shepherd, 1996; Tuthill and Wilson, 2016b).

We tested the expression patterns of the selected lines in sensory neurons by visualization of mVenus tagged to the light-gated channel CsChrimson used in subsequent experiments (Wu et al., 2016). We observed that MsB1 neurons project to the ventral-most layer of the three leg Neuropils, the ventral association center (VAC) (Court et al., 2020) (Fig. S1). Conversely, the medial ventral association layer (mVAC) and the intermediate Neuropil (IntNP) received projections from ChO1 line neurons (Court et al., 2020) (Fig. 1 and S1). In the central brain we identified ChO1 axon terminals in the Wedge (WED) and AMMC consistent with the previously identified ChO primary neuron projections to the central brain (Fig. S1). The MsB1 line showed some labelling in the Antennal lobes and GNG, possibly axon terminals from head appendages (Gao et al., 2000; Kain and Dahanukar, 2015; Tsubouchi et al., 2017). After close inspection of the head appendages

145 we found cell labelling in the maxillary palps, in the proboscis and in the 3rd antennal
146 segment (Fig. S1 and data not shown).
147 Next we measured the behavioral responses of immobile flies to optogenetic stimulation
148 of these 2 classes of sensory neurons. For this we drove the expression of the light-gated
149 CsChrimson channel in the respective structures and analyzed the flies' behavior after a
150 single 100 ms stimulation in an open field arena (see Methods). While control Empty-
151 GAL4 flies remained immobile immediately after stimulation, eventually resuming motor
152 activity, the stimulation of leg mechanosensory Bristles or the leg femoral ChO led to
153 movement (Fig. 1D and Video S1). Motor responses differed between these two lines,
154 with MsB1 stimulation inducing a very short latency response, reaching a maximum
155 speed of 7.38 ± 1.17 mm/s, 60 ms after stimulus onset, while ChO1 stimulation led to a
156 more progressive response reaching maximum speed of 6.98 ± 1.99 mm/s after 1.6
157 seconds (Fig. 1D' and D'', upper panels). Moreover, MsB1 stimulation triggered a fast
158 startle response followed by sustained walking (Fig. 1D').
159 The different responses to optogenetic stimulation between ChO and MsB stimulation
160 suggested that these neurons promote movement by different neuronal circuits. We then
161 asked if movement initiation was dependent on descending information, by decapitating
162 the animals before optogenetic stimulation (Fig. 1E). Decapitated Drosophila are capable
163 of maintaining an upright posture and display innate behaviors such as grooming
164 (Hampel et al., 2017; Vandervorst and Ghysen, 1980).
165 Control animals (empty-GAL4) did not exhibit any optogenetic response, maintaining an
166 upright posture with occasional grooming behavior (Fig. 1E and data not shown).
167 Strikingly, MsB1 stimulation triggered a startle response and sustained motor activity for
168 approximately 2.9 seconds (Fig. 1E' and Video S1). Moreover, under these conditions,
169 animals reached a peak speed of 6.85 ± 1.27 mm/s, 60 ms after stimulus onset, similar to
170 the one observed in head-intact animals, indicating that the initial response to
171 mechanosensory stimulation is mediated by circuits located within the VNC, independent
172 of descending circuits. In contrast, ChO1 stimulation in beheaded flies did not induce
173 movement initiation (Fig. 1E''), indicating that these sensory neurons activate central
174 brain circuits that in turn are responsible for walking initiation. Optogenetic stimulation
175 of ChO1 in decapitated flies did however lead to a reflexive leg twitch, which induced a

176 small increase in the perceived instantaneous speed (arrow in Fig. 1E''and Video S**1**).
177 This reflex is most likely the consequence of direct synaptic connections between the
178 ChO and leg motor neurons, as described in locusts (Burrows, 1996; Burrows et al.,
179 1988; Kittmann and Schmitz, 1992; Tuthill and Wilson, 2016a).
180 These results indicate that stimulating mechanosensory structures in the leg is sufficient
181 to induce walking initiation, which in the case of MsB only depends on local circuits
182 within the VNC. However, sustained walking after MsB stimulation requires descending
183 activity from the head.
184
185 **MsB stimulation evokes movement encompassing a non-coordinated phase**
186 Having shown that MsB stimulation triggers walking response in head intact flies, we
187 next investigated the kinematic features associated with this motor response. For this we
188 used the FlyWalker system that allows the quantification of kinematic parameters with
189 high spatial and temporal resolution generating a large set of outputs including step,
190 spatial and gait parameters (Cabrita et al., 2022; Mendes et al., 2013; Mendes et al.,
191 2014)**.** The walking chamber was modified in order to accommodate a far-red LED array
192 to perform optogenetic stimulation where each fly received one pulse of 100 ms red light
193 stimulation and the resulting behavior was quantified.
194 Control animals display a typical gait pattern showing an alternating tripod configuration
195 (Fig 2A) and consistent stance traces (Fig 2C), which mark the tarsal contacts relative to
196 the body axis during stance phases, indicating high levels of leg coordination under these
197 conditions (Burrows, 1996; Mendes et al., 2013; Strauss and Heisenberg, 1990; Wosnitza
198 et al., 2013)**.** Forward movement induced by leg MsB stimulation can be classified into
199 two distinct phases using visual inspection of the step patterns: an early *uncoordinated*
200 *phase* followed by a late *coordinated phase* (Fig. 2B/D and B'/E, respectively; and Movie
201 S2). The *uncoordinated phase* immediately follows optogenetic stimulation, displaying
202 an apparent random step pattern without any clear coupling between the six legs, leading
203 to an inefficient force transduction that results in a slow and non-cyclic movement (Fig.
204 2B). We further analyzed the step configurations, a proxy for inter-leg coordination, and
205 found a large proportion of frames that do not match any of the normal gaits or
206 configurations described by control flies, such as tripod or tetrapod (Mendes et al., 2013;

Strauss and Heisenberg, 1990; Szczecinski et al., 2018; Wosnitza et al., 2013) (Fig. 2B, lower panel). We describe these configurations as '*non-compliant*' since these do not conform with the rules of coordinated movement described by Durr et al. (Durr et al., 2004). Non-compliant configurations include, for example, two contralateral or two consecutive ipsilateral legs lifted simultaneously, which creates static instability. We observed that non-compliant configurations are used to a striking degree during the uncoordinated phase, ranging from 20% to 50% (average of 29.6±4.4%) of the frames compared to being nearly absent in control animals (Fig. 2F and H). This shift in gait pattern is matched by a reduction in the use of the canonical tripod and tetrapod gaits (Fig. 2H). These data suggest that stimulation of leg MsB induces activation of motor activity lacking inter-leg coordination. Moreover, stance traces display an extremely uncoordinated pattern with highly variable and inconsistent leg contacts, highlighting a lack of control and coordination during this phase of locomotion (Fig. 2B and D), even though leg retraction shows the typical anterior to posterior movement (Fig. 2D). Nevertheless, the high degree of uncoordinated movement suggests that in addition to a lack of inter-leg coordination, the proper coupling between leg segments (or intra-leg coordination) is lost during this initial phase of locomotion. We evaluated the whole kinematic profile and found that virtually all kinematic parameters were altered, with the notable exception of the average swing duration (Fig. 2H). Interestingly, we found that animals shifted from an uncoordinated phase to a distinct coordinated phase without requiring a transitional stop (Fig. 2B and B'). Nevertheless, during the transition most flies displayed a period during which all legs were in a stance phase, contacting the ground (19 out of 21, corresponding to 90.4%) (Fig. 2B, ~1.4s). From a total of 21 flies tested, 10 (48%) shifted to coordinated walking without stopping (see for example, Fig. 2B to 2B'), 4 (19%) shifted to coordinated walking after a small pause of 200 to 400 ms and 6 (29 %) of the flies initiated grooming for a significant period of time before resuming walking. During the coordinated phase the fly adopts mainly tripod and tetrapod gaits while non-compliance configurations are absent (Fig. 2B', lower panel). Once animals have returned to a coordinated phase, both gait patterns and stance traces display a pattern similar to control animals (Fig. 2H, 2B' and E). Kinematic parameters in the coordinated phase are more concordant with the standard walking pattern seen in

238 control animals although the recovery is not total, indicating that transient sensory
239 stimulation can have sustained effects on locomotion (Fig.2H, 2B').
240 In summary, stimulation of leg MsB results in a reflexive forward cyclic movement,
241 during which flies display an uncoordinated phase, lacking inter-leg coordination,
242 followed by a coordinated phase presenting the stereotypical properties of walking
243 animals.
244
245 **Kinematic features after leg MsB stimulation in headless flies**
246 We next investigated the kinematic features of headless flies upon leg MsB stimulation
247 (Fig. 3), which we previously found initiates locomotor behavior in the open arena setup
248 (Fig. 1 E). As described for Figure 2, we optogenetically stimulated leg MsB1 in an
249 enclosed arena and extracted kinematic features using the FlyWalker system (see
250 Methods). Prior to stimulation, we decapitated the flies and glued the heads back to the
251 thorax to allow proper body tracking by the FlyWalker software.
252 Stimulated flies display cyclic leg movements with a highly uncoordinated gait pattern
253 and stance traces (Fig. 3A, B). Moreover, kinematic properties also display a starkly
254 different profile compared to control animals (Fig. 3C). Noticeably, there is a similarity
255 between the walking pattern of the uncoordinated phase of the head intact flies and the
256 headless flies after stimulation (Fig. 3C). In fact, the stance straightness index is
257 indistinguishable between these two conditions (Fig. 3D, compare Fig. 2B' with 3B).
258 However, we observed that the time headless flies spend moving after the stimulus is
259 longer compared to the uncoordinated phase in head intact flies (Fig. 3E), suggesting that
260 descending circuits can interrupt the uncoordinated cyclic activity triggered by leg MsB
261 and mediate a transition to a coordinated walking pattern.
262 We then asked if descending control could influence the response to leg MsB stimulation
263 by comparing the early response in head intact animals to the response in headless flies.
264 First, we noticed a larger fraction of frames spent in a non-compliant configuration (Fig.
265 3F), which could be explained by a sustained swing phase during the initial stages of the
266 motor response (Fig. 3A, below ~1 sec, compare lower section, Fig. 2B with 3A).
267 Second, we subjected all the kinematic parameters to a Principal Component Analysis
268 (PCA) selecting the top 3 axes that explained most variance, thus yielding a three-

269 dimensional space representation (Fig. 3G). PC1, which explained the highest variance of
270 the data (50.2%), allowed a statistical discrimination between headless animals and the
271 uncoordinated phase in head-intact animals, with the cloud of points of headless animals
272 lying further away from control animals in the behavioral space (Fig. 3G' and G''),
273 suggesting that higher order circuits can influence the cyclic motor activity triggered by
274 leg MsB.
275 These data indicate that leg MsB can trigger sustained cyclic motor activity using solely
276 circuits within the VNC, albeit with severely impaired coordination between legs and leg
277 segments. This cyclic activity is nevertheless modulated and ultimately restrained by
278 central brain circuits and descending information.
279
280 **Inter-joint coordination is partially disrupted after MsB stimulation**
281 To further explore the disruption of coordinated locomotion following leg MsB
282 stimulation, we examined intra-leg, or alternatively called inter-joint coordination, i.e. the
283 correct modulation of joint angles within a single limb in relation to one another, required
284 to produce efficient walking (Cruse and Bartling, 1995). To extract measures of joint
285 angles we tethered flies expressing CsChrimson in leg MsB to a wire while they walked
286 freely on a polystyrene ball (Barrios et al., 2021; Buchner, 1976; Götz and Wenking,
287 1973; Seelig et al., 2010) (Fig 4A). As above, one 100ms light stimulation pulse was
288 delivered while the flies were immobile. Fly behavior was imaged using a lateral camera
289 at 120 fps and videos were tracked using DeepLabCut (Mathis et al., 2018), which
290 allowed us to extract 3 joint angles: 1) Coxa-Femur joint, 2) Femur-Tibia joint, 3) Tibia-
291 Tarsus joint (Fig. 4A, B and Video S3). We only considered angles from the T1 leg, since
292 this leg is predominantly at a perpendicular angle to the imaging path and thus the angles
293 could be accurately calculated in a 2D video. As expected from our earlier results, MsB
294 stimulation induced movement in both head-intact and headless flies (Fig. 4B, Video S3).
295 To determine whether inter-joint coordination was perturbed by the stimulation protocol
296 we compared 4 conditions: walking flies (*pre-stimulation*) (Fig. 4B, top panel); head-
297 intact flies for the initial 1s after stimulation onset (termed "*early response*") (Fig. 4B,
298 middle panel, red section); head-intact flies 3-5s after stimulation onset (termed "*late*
299 *response*") (Fig. 4B, middle panel, green section); and headless flies for the first 1s after

stimulation onset (termed "*headless response*") (Fig. 4B, lower panel, purple section). We chose these time periods to capture the 'uncoordinated' and 'coordinated' phases of post-stimulation movement previously described (Figs. 2 and 3).

As expected, *pre-stimulation* walking flies showed stereotyped periodic patterns of joint angles (Feng et al., 2020) (Fig 4B). The Coxa-Femur joint and the Femur-Tibia joint were strongly modulated throughout the step-cycle in a correlated fashion, whilst the Tibia-Tarsus joint did not show an obvious correlation to the step cycle. We performed a Fast Fourier Transform (FFT) to extract component frequencies from the data (Fig. 4C). In *pre-stimulation* walking flies, the Coxa-Femur and Femur-Tibia joints showed the highest power at 7.0 Hz, corresponding to the average step frequency (Fig. 4C and Fig. S3A), while the Tibia-Tarsus joint was not periodically modulated (Fig. S3A). FFT analysis of the *early-response*, *late-response* and *headless response* also showed that Coxa-Femur and Femur-Tibia joints were more strongly modulated than the Tibia-Tarsal joint (Fig. S3A). We thus restricted our subsequent analysis to only Coxa-Femur and Femur-Tibia joints. To understand the regularity of motor behavior following stimulation we compared the FFT of our 4 conditions for the Coxa-Femur joint (Fig. 4C). Whilst in the intact-early stage the strong periodic modulation of joint angles seen in walking flies is lost, by the late stage, a peak has re-emerged (albeit around 5.2 Hz, a lower frequency than in the walking condition), showing the angles traces are once more becoming structured. Strikingly in headless flies, frequencies were highly variable with no clear peaks (Fig. 4C).

To further investigate the relationship between joints, we generated angle-angle plots between the Coxa-Femur joint and the Femur-Tibia joint for our 4 conditions (Fig. 4D). Angle-angle plots for walking flies showed a half moon-shaped 'ring' trajectory (Fig. 4D), corresponding to the stance and swing phases of the step cycle (Fig. S3B). Angle correlations were altered in the *early response* following stimulation (Fig. 4D). Whilst the half-moon outline was still visible, indicating that the fundamental relationship between joints has not been totally lost, the variability of the movement was greatly increased. Under *late response* conditions (i.e. 3-5 seconds after the stimulation) traces once more display a regular 'walking-like' ring (Fig. 4D). However, during *headless response* conditions, very distorted angle-angle traces are visible with an undetectable ring pattern.

To quantify dispersion from the average walking cycle, we calculated the mean trace of the walking angles (Fig. 4D, black lines and Fig. S3B). We then analyzed the minimum distance for each measured point to the mean trace (Fig. 4E, F). Distances were significantly increased for all stimulated conditions as compared to pre-stimulus condition (Fig. 4F), indicating a significant disruption of the co-ordination between joints after MsB stimulation ($P_{walking\text{-}early\ response} < 0.001$, $P_{walking\text{-}late\ response} < 0.001$, $P_{walking\text{-}decapitated} < 0.001$, Dunn's test). Distances were reduced from the *early response* to the *late response*, indicating a partial recovery of coordination ($P_{early\ response\text{-}late\ response} < 0.001$, Dunn's test). In contrast, distances were greatly increased in the headless condition, indicating that loss of brain control leads to wildly disrupted relationships between joint angles ($P_{early\ response\text{-}decapitated} < 0.001$, $P_{late\ response\text{-}decapitated} < 0.001$, Dunn's test). To understand which aspect of the relationship between angles was disrupted, we divided the angle-angle space into 4 quadrants (described in Fig. S3C). The positions of the lines were chosen to split the walking traces into 4 components of the step cycle – stance onset/quadrant 1 (corresponding generally to high Coxa-Femur angles); stance offset/quadrant 2 (corresponding to low Femur-Tibia angles); swing onset /quadrant 3 (corresponding to low Coxa-Femur angles); and swing offset/quadrant 4 (corresponding to high Femur-Tibia angles). We calculated the proportions of data points which fell in each quadrant for each condition (Fig. 4G). Pre-stimulus walking flies spend more time in quadrants 1 and 2, corresponding to the slow stance phase, and less time in quadrants 3 and 4 which correspond to the faster swing phase. Flies immediately after stimulation show an increase in occupancy of quadrant 3, likely corresponding to aborted swing initiations. Strikingly, headless flies show a large over-representation of points in quadrant 4, corresponding to extended Femur-Tibia angles, indicating that without descending control, extension is the default response, indeed to an extent where the flies almost invariably let the ball fall (Video S3). This effect was also observed in the gait-analysis experiments (Fig. 3 and Video S2).

Overall, our data show that inter-joint coordination is partially lost immediately after stimulation in head-intact flies, but has begun to recover by the period of 3 – 5 seconds after stimulation. In contrast, joint angles are highly uncoordinated following stimulation in headless flies, which show large overextensions of the Femur-Tibia joint, suggesting a

362 role for descending control to appropriately regulate the relationships of joint angles to
363 one another.
364
365 **Intra joint muscle coordination is maintained during movement triggered by MsB**
366 Key for coherent locomotor activity is the reciprocal inhibition of opposing flexor and
367 extensor muscles, each one controlled by their respective excitatory motor neuron pool
368 (Eccles et al., 1956; Grillner, 1975; Sherrington, 1893). This implies that contraction of
369 one joint muscle is concurrently matched by relaxation of its antagonistic muscle within
370 the same joint. We asked if sensory-triggered movement also follows this muscle pattern,
371 which we refer as intra-joint coordination. For this we monitored muscle contraction at
372 the femur-tibia joint by measuring GCaMP fluorescence in leg muscles while
373 optogenetically stimulating Leg MsB (Fig. 5A) (Heredia et al., 2021; Soler et al., 2004),
374 see Methods). The fly's body and legs were glued to a coverslip (Kamikouchi et al.,
375 2010), and muscle activity in the femur was recorded using a spinning disc confocal
376 while the fly was stimulated with a 100ms light stimulus (see Methods). We identified the
377 femur extensor and flexor muscles (Fig. 5B) and quantified the percentage of
378 fluorescence in each frame, normalized to the maximum and minimum of the
379 fluorescence for each video (Fig. 5B-D) (see Methods). In addition, we generated a
380 kymograph covering both extensor and flexor muscles (Fig. S4). As expected in head
381 intact flies, both controls groups (flies without stimulation and stimulated without all-
382 trans-retinol (ATR)-supplemented food) display alternating muscle activity, meaning that
383 antagonistic muscles were not active simultaneously (Fig. 5C, left and middle panel and
384 kymograph on Fig. S4B). We calculated the Spearman correlation between the two
385 muscle signals over time, which generated negative values confirming their anti-phasic
386 relation (Fig. 5E). Optogenetic stimulation of leg MsB showed a fast muscle response in
387 accordance with the locomotor behavior previously observed. Interestingly, the observed
388 muscle activity maintained the antagonistic alternation seen in control flies (Fig. 5C right
389 panel, E and Fig. S4B). Stimulation of headless flies also led to an immediate muscle
390 contraction showing an alternating antagonistic muscle activity, albeit with a higher
391 variability (Fig. 5D, E). Notably, both in head-intact and headless animals, we found no
392 flexor or extensor muscle bias upon sensory stimulation (Data not shown), suggesting

393 that no particular muscle was more responsive to sensory stimulation and that indeed a
394 reciprocal motor pool inhibition mechanism is present to prevent muscle co-contraction
395 upon stimulation (Brown, 1911 ; Eccles et al., 1956). We also compared the GCaMP
396 fluorescence profile during muscle contraction by measuring peaks intensities and widths
397 (Fig. 5F-H, see Methods). Noticeably, stimulation of leg MsB in headless flies led to a
398 weaker muscle contraction pattern compared to head intact conditions (Fig. 5G),
399 suggesting that higher order centers may act as modulators of motor neuron recruitment
400 and activity. However, no differences were observed in the width of the muscle
401 contraction peaks between head intact and headless flies (Fig. 5H).
402 Overall, our results show that leg MsB stimulation evoked movement largely maintains
403 intra-joint muscle coordination properties in head-intact and headless flies.
404
405 **Cyclic movement triggered by MsB is leg specific**
406 Full body stimulation of mechanosensory bristles (using dust particles or genetically) has
407 been shown to trigger grooming behavior (Hampel et al., 2017; Seeds et al., 2014), while
408 in our study where we limit activation to just leg MsB, we found mostly uncoordinated
409 walking to be the main response. It has been suggested that compartmentalized sensory
410 connections mediate different behavioral responses (Siegler and Burrows, 1986;
411 Vandervorst and Ghysen, 1980). We thus asked if the motor response could be
412 determined by the body structure from which the stimulus originates. To target
413 expression of CsChrimson to MsB in other body segments, we used the same GAL4
414 driver but instead combined with a head capsule or wing-specific flp line using the
415 eyeless (ey) and vestigial (vg) fragments, respectably (Fig. 6A, see methods). We
416 confirmed the effectiveness of this approach based on the presence of positive cells in the
417 respective cuticle and axonal projections (Fig. S1). We then cataloged the repertoire of
418 motor behaviors in response to optogenetic stimulation using manual and automatic
419 classifiers (see Methods). These included uncoordinated and coordinated movement, leg
420 cycling and grooming.
421 As previously shown, leg MsB activation triggered uncoordinated displacement,
422 immediately followed by coordinated walking and grooming in some animals (12 out of
423 20) (Fig. 6B). Notably, wing and head stimulation did not induce uncoordinated

424 movement, with animals instead displaying coordinated walking (Fig. 6C-E), showing
425 that the uncoordinated activation of leg motor centers is specific to leg afferents.
426 Moreover, stimulation of wing MsB led only a small fraction of the animals to groom (2
427 out of 20) compared to leg or head stimulation (11 and 10 out of 20, respectively) (Fig.
428 6B-E), further highlighting the specificity of sensory stimulation for motor selection. This
429 suggests that behavior selection (in this case grooming) is dependent on the place where
430 the stimulus is received.
431 We then asked if the aforementioned behaviors are dependent on the presence of higher-
432 order brain commands. As observed previously, leg MsB stimulation in headless animals
433 caused uncoordinated body displacement (Fig. 6F and H). Additionally, close inspection
434 of the movies revealed an extra behavior, which is interestingly absent in head intact
435 animals: sustained random leg movements (Figs. 6F, brown sections and Video S4).
436 These movements do not display any synchrony between legs, thus rendering the fly
437 immobile.
438 Our data also show that the walking behavior triggered by the stimulation of wing MsB is
439 dependent on the presence of higher-order brain commands. Stimulation of wing MsB
440 afferents in headless flies did not induce walking or uncoordinated movement (Fig. 6G,
441 H), but instead grooming, (a behavior which is absent in head intact conditions (Fig. 6C),
442 suggesting a descending inhibitory command that blocks the grooming behavior). Video
443 analysis of headless flies showed that the observed leg movement bouts resembled the
444 preparatory pose for grooming (data not shown), or in some cases a defensive kick
445 behavior described previously to remove fictitious parasites (Li et al., 2016) (Video S4).
446 Overall, our data show that the motor response triggered by sensory stimulation depends
447 not only on the class of proprioceptors (MsB), but also on the source of the stimulus.
448 These data also highlight the role of the central brain controlling VNC pre-motor centers,
449 while executing particular leg motor commands such as leg twitching or grooming.

450

451 **Mechanosensory-triggered movement is dependent on the number of cells**

452 Leg mechanosensory bristles are present on the surface of the entire leg of the fly, with
453 neurons present in the most distal part of the leg projecting their axons to the central part

454 of the leg neuropil while neurons occupying proximal positions project to more
455 peripheral areas (Tsubouchi et al., 2017). Leg MsB display a concentric organization in
456 the leg neuropil instead of a concentrated topographical distribution within the VNC
457 (Tsubouchi et al., 2017). Since we showed that uncoordinated movement is evoked
458 specifically by leg MsB, we conjectured the possibility that a discrete subpopulation of
459 leg cells could be sufficient to activate the downstream motor program that triggers cyclic
460 movement, or alternatively, that the response results from the contribution of all leg MsB
461 being activated. To test these possibilities, we used 6 additional GAL4 lines to drive the
462 expression of CsChrimson in different bristles subpopulations in the fly leg, which we
463 called MsB2 to 7 (with our original line termed MsB1), ordered by the number of cells
464 labeled, with MsB1 the most and MsB7 the least. For each line we quantified number of
465 MsB labeled and looked at their localization in specific leg segments (Fig. 7A, B and
466 Table S1). We also measured the response of the different lines to optogenetic
467 stimulation by registering the duration of motor activity and categorizing the different
468 motor outputs in an open field arena (Fig. 7C and D, respectively). As previously
469 described (Fig. 1) the MsB1 line, which expressed GAL4 in 169 bristles in all leg
470 segments, had a strong reaction to the stimulus, showing motor activity for up to 1.5
471 minutes (Fig. 7C). Interestingly, stimulation of a lower number of cells in MsB2-6, which
472 label between 57-26 neurons, still triggered a motor response but with a shorter time span
473 (Fig. 7C), whilst MsB7, which drives expression in just 4 cells in the tarsal segments,
474 triggered minimal motor activity, suggesting that the duration of movement is influenced
475 by the number of activated cells. To further analyze the type of behaviors triggered by
476 mechanosensory bristles stimulation, we used the same behavioral classifier previously
477 used to identify immobility, body displacement, grooming, and sporadic leg movement
478 (Fig. 7D, E and S5). We observed that most lines show uncoordinated walking behavior
479 followed by sporadic leg movement without displacement. Some flies also displayed
480 grooming behavior, consistent with previous observations (Hampel et al., 2017) (Fig. 7D,
481 E). We also considered if particular leg segments are more responsive to the optogenetic
482 stimulus. Although we could not find lines specific to any particular segment at
483 comparable numbers, we noticed that activating the 57 tibial MsB in line MsB2 triggered
484 a shorter and less robust response compared to other lines, which labelled fewer, but

485 more proximally located, cells such as MsB3 and MsB5 (Fig. 7C-E, S5C), hinting at the
486 possibility that cells in proximal segments can trigger a more robust response to
487 mechanosensory stimulation.
488 These results suggest that no particular population of MsB is uniquely responsible for
489 inducing VNC-dependent leg movement but instead the cyclic motor response is due to
490 the cumulative stimulation of multiple MsB broadly distributed circuit in the VNC.

491 **Discussion**

492

493 In this study we took advantage of the sophisticated *Drosophila* genetic toolkit and
494 kinematic analysis tools to understand mechanosensory evoked motor responses in
495 different body regions. We found that a short 100-millisecond (ms) optogenetic
496 stimulation of two different leg mechanosensory structures is sufficient to initiate forward
497 movement in immobile animals (Fig. 1). In particular, MsB stimulation led a two-phase
498 motor response comprised by an immediate *uncoordinated phase* followed by a late
499 *coordinated phase* (Fig. 2; Video2). While the coordinated phase shows all the
500 fundamental features of normal locomotion, the uncoordinated phase lacks both inter and
501 intra-leg coordination whilst sustaining antagonistic antiphasic muscle activity (Fig.2, 4
502 and 5). Moreover, the uncoordinated phase is mostly dependent on spinal circuits as leg
503 MsB stimulated headless flies largely phenocopy the *uncoordinated phase* present in
504 head-intact animals (Fig.3, 4 and 5). Finally, we show that the motor response to MsB
505 stimulation is dependent on the segment and number of cells being stimulated (Fig. 6 and
506 7).

507

508 **Motor activity by targeting of Spinal Motor Circuits**

509 This study unveils a new circuit for direct activation of VNC locomotor neural networks.
510 The stimulation of MsB leads to the direct engagement of spinal circuits without
511 interference of the central brain, resulting in a forward movement that lacks inter-joint
512 and inter-leg coordination but still maintains intra-joint coupling.

513 Previous studies have shown the generation of motor programs through the stimulation of
514 sensory structures. For example, the mechanical and optogenetic activation of bristles in
515 the entire body of the fly are able to elicit grooming movements (Hampel et al., 2017),
516 whereas the activation of specific bristles on the wing margin, which could be caused by
517 an invading mite, leads to the initiation of a directed kick towards the stimulated area (Li
518 et al., 2016). Importantly, these sensory-triggered behaviors are still maintained in
519 headless flies. These data highlight that the circuits required for the processing and
520 execution of ethologically relevant behaviors are present in the VNC, which can be
521 executed with remarkable speed and precision. Likewise, our data present evidence that

522 neural networks in the VNC are capable of processing leg mechanosensory feedback to
523 execute the appropriate cyclic motor program. Moreover, this response is not exclusively
524 due to the activation of MsB but also depends on the origin of the stimulus. Notably,
525 stimulation of wing MsB did not induce uncoordinated walking but mostly grooming and
526 kicking as previously described (Hampel et al., 2017; Li et al., 2016) (Fig. 6). These data
527 support that the location of the sensory input plays a major role in the selection of the
528 motor outcome, instead of solely the class of the mechanosensory structures conveying
529 the stimulus. Since the leg and wing MsB target distinct neuropil regions in the VNC,
530 namely the leg and wing neuropils (Tsubouchi et al., 2017) (Fig. S1), respectively, it is
531 thus likely that distinct and possibly non-overlapping motor circuits become active.
532 While the grooming and kicking behavior after bristle stimulation are important for the
533 fly to rid itself of invading parasites and debris, the uncoordinated forward movement
534 here does not follow the same purpose. Instead, this behavior could be an escape response
535 caused by inter-fly contacts or other imminent threats (Ramdya et al., 2015). This
536 response is analog to the jump reflex, a behavior triggered by visual stimuli that activates
537 the giant fiber – a large descending interneuron synapsing directly on the mesothoracic
538 neuromere (T2) motor neurons leading to a jump and flight takeoff (King and Wyman,
539 1980; Tanouye and Wyman, 1980; Trimarchi and Schneiderman, 1995)}. However, we
540 should point out an important distinction between giant fiber and leg MsB stimulation:
541 while stimulation of the giant fiber induces a reflexive tonic response from the ipsilateral
542 tergotrochanteral muscle (TTM) leading to a jump reflex (King and Wyman, 1980); MsB
543 stimulation leads to a motor program comprised of sustained alternating antagonistic
544 muscle activity.
545
546 **Sustained activity and segmental coupling**
547 In this study, the movement evoked by the stimulation of MsB shows characteristic CPG-
548 like activation, where antagonistic muscles maintain anti-phasic contraction leading to
549 joint movement (Büschges et al., 1995; Fuchs et al., 2011; Pearson, 1972; Ryckebusch
550 and Laurent, 1993) (Fig 5). The same behavior was observed in headless flies, implying a
551 lack of interference of ascending or descending neurons in the sensory-evoked
552 movement. These results are similar to the pharmacological stimulation of decapitated

553 flies with stimulatory amines, notably serotonin, dopamine, and octopamine, which lead
554 to locomotor bouts (Yellman et al., 1997). Moreover, studies in deafferented VNCs using
555 the muscarinic cholinergic agonist pilocarpine, have shown alternating and rhythmic
556 activity in antagonistic leg motor neuron pools driven by the CPGs (Bidaye et al., 2018;
557 Büschges et al., 1995; David et al., 2016; Fuchs et al., 2011; Goldammer et al., 2018;
558 Pearson, 1972; Ryckebusch and Laurent, 1993). Despite this large body of work, the
559 identity, location and architecture of the CPG population remains largely elusive. The
560 reason for this gap in knowledge is the difficulty in accessing the neuronal VNC
561 population, adding to the problems in separating the outputs from CPG and the activity in
562 neurons that process sensory information during stepping. Nevertheless, some
563 interneurons were identified as being part of this network in the cockroach and in the
564 stick insect (Bassler and Buschges, 1998; Pearson and Fourtner, 1975). The use of
565 mechanosensory stimulation in the fly provides an attractive port of entry in order to
566 further identify and perform physiological characterization of leg CPGs taking advantage
567 of the expanding Drosophila genetic toolkit (Meissner et al., 2022). The second-order
568 neurons from the mechanosensory fields remain elusive, although data from the locust
569 suggest that these afferents target spiking local interneurons, some of which synapse on
570 motor neurons (Siegler and Burrows, 1986). The reconstruction of serial-section electron
571 microscopy (EM) datasets from the *Drosophila* VNC will provide a detailed connectome
572 profile of the leg MsB (Phelps et al., 2021).
573
574 **Cyclic activity and intersegmental coordination**
575 Remarkably, we found reduced intersegmental coordination between hemi segments and
576 leg joints immediately after MsB stimulation (Figs 2-4), albeit with antagonistic muscle
577 contraction still being maintained (Fig. 5). These data resemble the effects of the
578 muscarinic agonist pilocarpine in deafferented insect VNC preparations, which generate
579 rhythmic activity of alternating motor neuron pools controlling joint movement (Baudoux
580 et al., 1998; Chrachri and Clarac, 1987; David et al., 2016; Goldammer et al., 2018;
581 Rillich et al., 2013; Ryckebusch and Laurent, 1993). Moreover, this rhythmic activity is
582 independent within the three leg joints, as these rarely exhibit coordinated activity
583 between them, meaning that different CPGs control the antagonistic activity of motor

584 neuron pools of each leg joint (Bidaye et al., 2018; Büschges et al., 1995; Daun et al.,
585 2019; Ryckebusch and Laurent, 1994). Given that in our experimental design, animals
586 still maintain their proprioceptive features that assist in segment coupling, we can
587 speculate that the MsB-dependent cyclic activity overrides or is insensitive to sensory
588 feedback or to any other coupling mechanism. Our data also suggest a role for
589 supraspinal feedback promoting segmental coordination since decapitation decreased the
590 degree of inter- and intra-leg coordination (Figs. 3F, G and 4F). Work on
591 hemimetabolous insects has shown a role for descending neurons (DNs) that traverse the
592 neck controlling the onset and features of walking patterns (reviewed by (Bidaye et al.,
593 2018; Strausfeld et al., 1984)). Moreover, optogenetic manipulation of defined
594 populations of DNs can trigger stereotyped behaviors and change walking patterns
595 (Cande et al., 2018; Namiki et al., 2018). Multisegmental coupling is provided either by
596 sensory feedback, descending inputs or centrally by nonspiking interneurons (Buschges,
597 1995; Juvin et al., 2012). The relevance of each component depends largely on the speed
598 the animal typically assumes, with slow-walking animals - such as the stick insect -
599 relying heavily on sensory feedback (Akay and Büschges, 2006; Akay et al., 2007;
600 Mantziaris et al., 2017). Regardless, our results suggest that, as in other insects,
601 alternating activity of antagonistic motor pools in *Drosophila* are uncoupled between
602 different joints and hemisegments, further reinforcing the use of *Drosophila* as a unique
603 model system to unravel the neuronal architecture responsible for coordinated motor
604 patterns.
605
606 **Implications for vertebrate systems /Clinical Applications**
607 Our study demonstrates that the stimulation of a specific sensory class has a direct effect
608 on the engagement of locomotor circuits in the VNC. These findings highlight the
609 possibility of using mechanosensory feedback circuits as a rehabilitation tool after spinal
610 cord injury. Regaining locomotor function after a spinal cord lesion requires the
611 reconnection of downstream locomotor circuits below the lesion and descending neurons
612 (Ballermann and Fouad, 2006; Bareyre et al., 2004; Rosenbaum et al., 2010). This can
613 happen through the growth and synaptic arborization of supraspinal and spinal projection
614 neurons leading to spontaneous recovery after incomplete spinal cord injury (Takeoka et

al., 2014). Post lesion studies show that mice deprived from sensory feedback exhibit poor reconnection of the descending circuits, leading to a lack of recovery and strong impairments in locomotion (Bareyre et al., 2004; Courtine et al., 2008; Takeoka et al., 2014). These loss-of-function results suggest that sensory feedback support the stabilization and rewiring of circuits deprived of upstream stimulation. Conversely, our data show that activation of specific sensory afferents are able to directly engage spinal motor circuits. Considering the evolutionary conservation of motor circuits, our results support the hypothesis that direct sensory electrical stimulation can foster the rewiring of injured circuits enhancing recovery outcomes (Capogrosso et al., 2013; Takeoka et al., 2014). In humans, targeted spinal cord stimulation improves locomotor performance in individuals with severe motor deficits or even leg paralysis (Angeli et al., 2014; Formento et al., 2018; Wagner et al., 2018). The direct stimulation of dorsal roots, where proprioception structures reside thus represents a more surgically accessible approach for the activation and recovery of paralyzed structures.

629 **Methods**

630

631 **Fly strains**

632 All flies used in this study were non-virgin females between 1 and 7 days post-eclosion.
633 Flies were housed in a 25° incubator with 50-70% humidity. Prior to experimentation, all
634 flies were manipulated under cold anesthesia and allowed to recover for at least 24h. The
635 GAL4 lines from the Janelia Flylight Collection were: R65D12-Gal4(attP2), R77E09-
636 Gal4(attP2), R85A07-Gal4(attP2), R45D07-Gal4(attP2), R54A11-Gal4(attP2), R39A11-
637 Gal4(attP2) and R64D07-Gal4(attP2), R50A05-Gal4(attP2), R22E04-Gal4(attP2),
638 R79E02-gal4(attP2) and pBDP-GAL4UW (w[1118];P{GAL4.1Uw}attp2) (EmptyGal4).
639 Ato1.9-flp and $Vg^{BE}$ -flp were generated by TOPO cloning into an entry clone the 1.9kb
640 enhancer fragment from the regulatory region of atonal (zur Lage et al., 2004), and the
641 boundary enhancer of vestigial ($Vg^{BE}$) (Williams et al., 1994; Zecca and Struhl, 2007) (a
642 gift from Mirian Zecca), respectively. Both entry clones were subjected to a Gateway
643 reaction into a flp destination plasmid. Transgenic lines were generated by standard
644 procedures in a *yw* background. The $dac^{RE}$-flp was used in previously (Mendes et al.,
645 2013). UAS-FRT-stop-FRT- CsChrimson-mVenus was a gift from Gerry Rubin (Wu et
646 al., 2016). UAS-FRT-stop-FRT-GFP, Lexop-GCaMP6f and ey-flp lines were obtained
647 from the Bloomington Stock Center. For the calcium imaging in leg muscles we used
648 lexO-GCamp6f/;mhc-lexA,lexO-Cherry/SM6ˆTm6b (Heredia et al., 2021) and the
649 recombinant line $Dac^{RE}$-flp;Uas-FRT-stop-FRT-CsChrimson-mVenus (VK5), R65D12-
650 Gal4 (attP2).

651

652 **Behavior Setup and optogenetic activation of mechanosensory structures**

653 The open field behavior arena for optogenetic stimulation was custom built from 3 mm
654 opaque white and black acrylic sheets using a laser cutter. The circular arena had a
655 diameter of 54mm, and was surrounded by 6 deep 655 nm red Leds (LUXEON Rebel
656 Led's) evenly distributed providing a stimulation power of 0.016 $mW/mm^2$ (Fig. 1C),
657 The edge of the arena was surrounded by water to prevent flies accessing the walls. The
658 top of the arena (transparent acrylic) was covered with Sigmacote (Sigma-Aldrich). A
659 white LED array was placed under the arena to serve as backlight. Flies were imaged

660 from above using a camera (Flea3-USB3, Point Grey, Teledyne FLIR LLC) equipped
661 with a 12 mm Computar (Commack, NY) lens covered with a 600nm, OD 4.0 Shortpass
662 Filter (Edmund optics, Barrington, NJ) to block optogenetic stimulation light.
663 For the experiments in Figure 1, we used 1-7 day old females, comprising 20 control flies
664 (empty-GAL4), and 20 flies expressing CsChrimson in leg mechanosensory bristles. Flies
665 were bred and kept in food infused with all trans-Retinal (Final Concentration 0.4 mM
666 ;R2500, Sigma-Aldrich). Single flies were aspirated into the chamber. We waited for a
667 spontaneous pause in behavior (no walking or grooming) and manually delivered a single
668 1-pulse stimulation of 100ms. Imaging continued for at least 20 seconds after stimulation.
669 For decapitated fly experiments, flies were anesthetized on a cold plate and their head
670 was cut off. After the surgery flies were kept in an empty vial for 1-5 minutes prior to
671 testing.
672
673 **Video acquisition and Tracking**
674 The video image was acquired at 30 Hz (1200 x 1210) using Fly capture software. Image
675 segmentation was performed by custom software in python using OpenCV. Two main
676 features were extracted from the videos: fly position (X and Y coordinates) and pixel
677 change around the fly. Positions were calculated from the centroid of an ellipse fitted to
678 the fly by background subtraction. The pixel change was quantified by calculating the
679 number of active pixels in a 100x100 pixel region surrounding the centroid. A pixel was
680 considered to be active if it recorded a change higher than 10 intensity levels.
681 The fly distance and speed were calculated for each frame using fly position x and y
682 coordinates with the formula:

$$distance = \sqrt{(x - x0)^2 + (y - y0)^2}$$

$$speed = \frac{distance}{time}$$

683
684 **Behavioral Classifiers**
685 We used velocity and pixel change features to automatically classify behavioral states.
686 We classified fly behavior into 4 categories: Walking, Grooming, Stopping and Leg
687 Displacement. A fly is considered to be walking if its average speed is higher than

688 1.9mm/sec. Grooming is detected when the velocity of the fly is lower than 1.9 mm/s and
689 average pixel change of a section of 8 frames is above 180 pixel/s. We classified as leg
690 displacement the movement in which velocity is lower than 1.9 mm/s and average pixel
691 change of a section of 8 frames is between 30 and 180 pixel/s. Finally, a fly is considered
692 to be stopping when velocity is lower than 1.9 and pixel change is lower than 30 pixel/s.
693 Thresholds were determined and confirmed by manual annotations of fly behavior (% of
694 efficacy). Later walking behavior was either classified into coordinated or uncoordinated
695 walking by visual inspection (Fig. 6 and 7).
696
697 **fTIR imaging and FlyWalker software**
698 For the analysis of walking behavior upon stimulation of sensory structures a new arena
699 comprising 12 LEDs (Deep red 655nm, Luxeon Rebel LED) was incorporated in the
700 previously described fTIR setup (Mendes et al., 2013), rendering a stimulation power of
701 0.014 $mW/mm^2$. Flies were placed in the FlyWalker arena and a 100 ms pulse of red light
702 was given. Each fly only received 1 pulse. The walking kinematics of flies after
703 stimulation were quantified using FlyWalker software package. One more parameter
704 called Non-Compliance Index was added to the previously published Kinematics
705 parameters. Non-Compliance Index is defined as the fraction of frames in a video in
706 which the fly displays non-compliant leg combinations. Non-canonical stance
707 combinations correspond to patterns that do not fit either of the idealized tripod, tetrapod
708 and wave gaits (Mendes et al., 2013; Mendes et al., 2014). In the experiments where we
709 used headless flies, we glued the head back onto the thorax using UV curable glue
710 (Loctite 3104, Henkel Adhesives) in order to avoid alterations in the body weight that
711 could potentially change walking patterns of the fly and to facilitate tracking.
712
713 **Tethered fly imaging**
714 For imaging of leg angles in Figure 4 we used 3-7 days-old females expressing
715 CsChrimson in mechanosensory bristles, as above. Adult flies were kept in food infused
716 with all trans-Retinal since the day of eclosion (Final Concentration 0.4 mM;
717 R2500,Sigma-Aldrich). Flies were anaesthetised on ice, and either decapitated with
718 scissors (Fine Scientific Tools) or left with head intact. They were positioned on a cold

719 plate with the thorax upwards, and a wire was glued to the thorax with UV curable glue
720 (Norland Optical Adhesives #81). Flies were fixed in the tethered set-up using the wire
721 above a porexpam ball (4.5 mm diameter, painted with black paint (Posca Uni)), held in a
722 custom made holder (the glass funnel of a Pasteur pipette). Flies could freely pick up and
723 walk on the ball, and if dropped could regain it again. Each fly was allowed to recover for
724 5 minutes on the set-up. After 5 minutes we waited for a spontaneous pause in behavior
725 and delivered a 100ms light stimulus via a single deep red LED (wavelength 627nm),
726 positioned 3 cm away from the fly. Light power at the fly was 13.8 nm/cm$^2$, calibrated to
727 produce a motor response in CsChrimson flies whilst not affecting flies in food lacking
728 all trans-Retinal (data not shown). Animals were illuminated with an InfraRed LED
729 (Thorlabs) and imaged with a PointGrey Camera (Flea3) with a Computar Macro-zoom
730 lens and a long-pass filter, at a frame rate of 120 fps. Video capture and LED stimulation
731 were controlled using a custom built Bonsai workflow (Lopes et al., 2015).
732 Walking bouts were extracted from head-intact non-stimulated flies (either before
733 stimulation or in sessions where no stimulation was delivered), and were manually
734 classified as satisfying straight walking with at least 6 step cycles. In total 8 walking
735 bouts were used from 3 flies. In the Head-intact and headless stimulation conditions for
736 the 'early response' and 'late response' timepoint, we visually inspected videos and
737 excluded timepoints where the flies were either still or performing grooming, as being
738 non-informative for our question of limb coordination while walking. Total N was 11
739 (head intact early response), 6 (head intact late response) and 10 (decapitated early
740 response). Videos were analyzed using DeepLabCut (Mathis et al., 2018). 18 points were
741 tracked in total; 3 body points (head, thorax and tail) and 5 points per leg (Body-Coxa;
742 Coxa-Femur; Femur-Tibia; Tibia-Tarsus; and Tarsus-end); however only T1 limb
743 tracking was used for the final analysis. Limb angles for T1 legs were calculated from
744 tracked positions using python.
745
746 **Leg and VNC dissection and Mounting**
747 To observe the morphology of leg sensory neurons, legs were dissected from the body in
748 PBS. The legs were then fixed in PFA 4% overnight at 4°C. After fixation legs were
749 washed 3x in 0.3% Triton-X in PBS for 20 minutes at R.T and mounted in 70% glycerol.

750 Brains and VNCs were fixed in PFA 4% for 20 minutes and dissected in PBS. Tissues
751 were labeled with a primary antibody raised against brp (mouse nc82, 1:10; DSHB)
752 followed by a secondary anti-mouse 647 (1:500; Jackson immunologicals). Tissues were
753 mounted in in 70% glycerol and scanned in a confocal microscope Zeiss (Oberkochen,
754 Germany) LSM710 confocal microscope with a 40× objective.
755
756 ***In vivo* calcium imaging during leg stimulation**
757 Flies containing the following genotype: lexO-GCamp6f;mhc-lexA,lexO-Cherry and
758 dacRE-flp;Uas-FRT-stop-FRT-CsChrimson-mVenus(VK5), R65D12-Gal4(attP2) were
759 anesthetized with ice for 3-5 min. Three ipsilateral legs were glued to a glass slide with
760 UV-Curable glue. The body of the fly was immobilized using beeswax. GCaMP imaging
761 was performed at 25°C on a Nikon/Andor Revolution XD spinning-disk confocal
762 microscope with an EMCCD camera (iXon 897) using iQ 3.5 software and using a 20×
763 CFI Super Fluor 20X 0.75 NA dry objective. Images were taken at the scan speed of
764 100ms per frame. A set of 6 deep red LEDs was paced around the fly to provide the
765 100ms red light pulse.
766
767 **Data processing and Analysis**
768 We extracted motor parameters using FlyWalker Software. Since many of the measured
769 gait parameters vary with speed, we analyzed the data for these parameters by
770 determining the best-fit regression model of each individual parameter with speed for the
771 control experiment and then determining the residual values for each experimental group
772 in relation to this regression model. Data was then expressed as the difference to the
773 residual normalized line. Normalized data was previously tested for normality and
774 homoscedasticity with Shapiro-Wilk and Levene tests. Statistical differences between
775 experimental groups were determined using Kruskal-Wallis analysis of variance followed
776 by Dunn's post hoc test (for non-normal distributions) or one-way-Anova followed by
777 Tukey's post hoc test (for normal distributions). Data analysis was performed using
778 custom Python scripts. Boxplots represent the median as the middle line, with the lower
779 and upper edges of the boxes representing the 25% and 75% quartiles, respectively.
780 Whiskers represent the range of the full data set, excluding outliers. Outliers are defined

as any value that is 1.5 times the interquartile range below or above the 25% and 75% quartiles, respectively. For the boxplots in fig 2 and 3 we decided to use raw data not normalized to the control since Non-Compliance index and Stance straightness parameters do not show a correlation with velocity (data not shown).

To have a more succinct representation of the data we used Principal Component Analysis (PCA), an unsupervised dimensionality reduction method. PCA finds a linear projection of the data from a high-dimensional space onto a lower-dimensional subspace, while maximizing variance of the projected data, and thus retains meaningful information, resulting in a description of the data as a function of a smaller set of uncorrelated variables (or principal components). The data were first pre-processed by centering and scaling, after which the PCA algorithm computed the covariance matrix in order to determine the correlation between variables and calculated the eigenvectors and eigenvalues of the covariance matrix in order to identify the principal components. We chose the first three principal components to visualize the data. The first two components were chosen to generate a two-dimensional plot. Each dot in the plots corresponds to a video, representing these new abstract variables. Color-coded dots were used to distinguish specific groups. As such, clusters of dots reflect similar walking patterns, shared by the corresponding flies (Cabrita et al., 2022).

For the analysis of the muscle fluorescence, we used Fiji software. To delineate the ROI Area of the depressor and levator muscle we used the threshold tool and measured the mean fluorescence value for each frame using ROI Manager, multimeasure tool. Fluorescence values for each muscle were normalized by subtracting the minimum value of each video and dividing by the maximum value, giving contraction values between 0 and 100%. Muscle contraction peaks were detected with a peak finding algorithm in Python. Peak width was calculated by subtracting fluorescence 20 percentage points from each peak value, and measuring the width of the signal that exceeded this value around each peak (Fig 4F).

## Figures

Figure 1

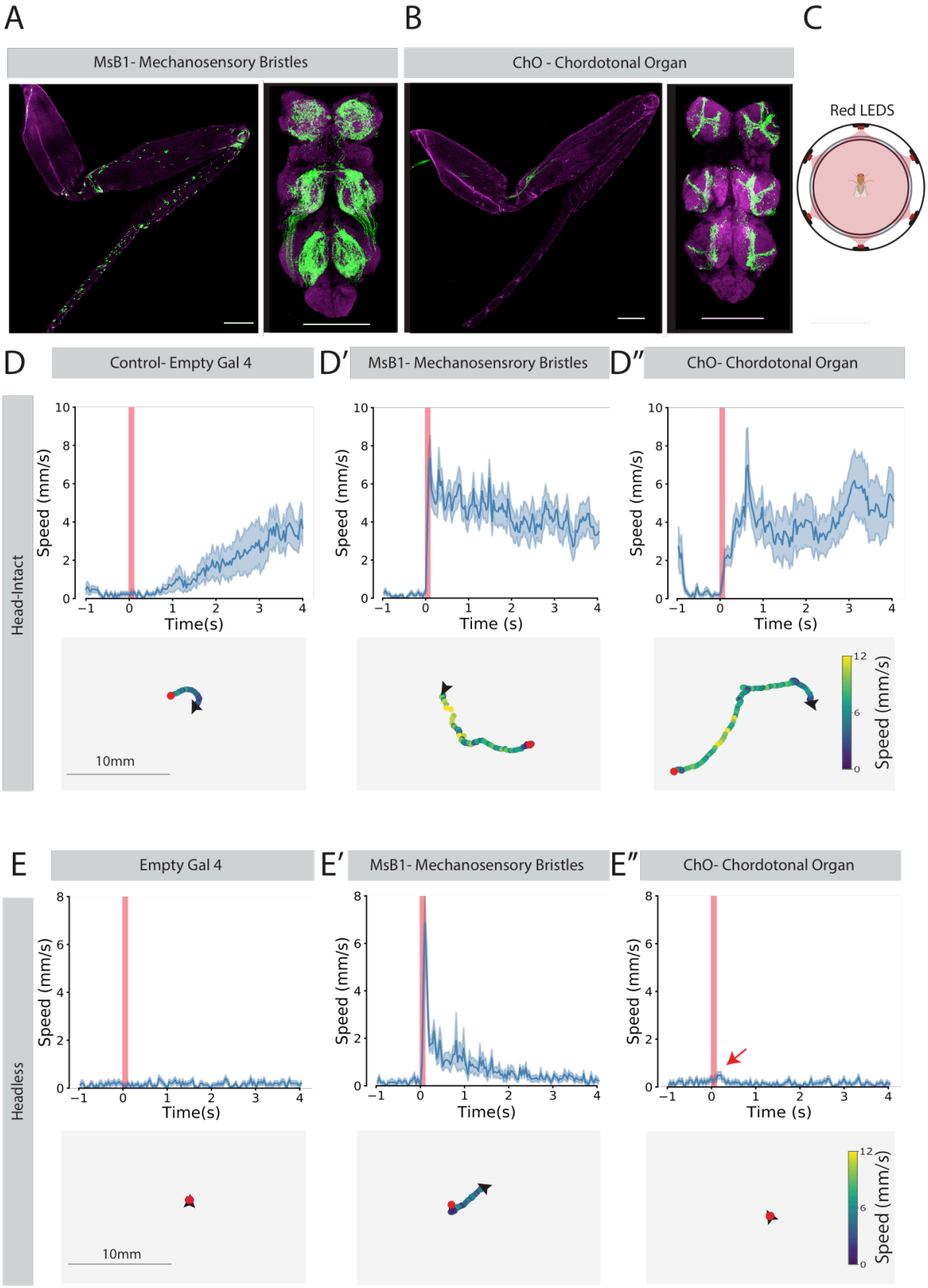

811 **Figure 1. Optogenetic stimulation of leg mechanosensory bristles triggers movement**
812 **in stationary flies**
813 (A) Leg and VNC expression pattern of leg MsB. mVenus expression under
814 combinatorial control of R65D12 and dac$^{RE}$-flp. Genotype: R65D12-GAL44, dac$^{RE}$-flp,
815 UAS-FRT-stop-FRT-Chrimson-mVenus. Cell bodies are located in the legs (left panel)
816 and send axonal projections to the VNC (right panel). Bar, 100 μm. (B) Leg and VNC
817 expression pattern in femoral ChO neurons. mVenus expression under combinatorial
818 control of R79E02 and ato-flp. Genotype: R79E02-Gal4, ato-flp, UAS-FRT-stop-FRT-
819 Chrimson-mVenus. Cell bodies are located in the legs (left panel) and send axonal
820 projections to the VNC (right panel). Bar, 100 μm. (C) Schematic of the behavioral arena.
821 Arena is surrounded by 6 deep red LEDs. See Methods for details. (D, E) Instantaneous
822 speed and trajectories over time after optogenetic stimulation. Upper panels show
823 instantaneous speed over time with red bar representing 100 ms red light stimulus. Dark
824 line and light blue shadows indicate the average and SEM for all replicates, respectively.
825 Lower panels show representative trajectories for 4 seconds after optogenetic stimulation.
826 Trajectory plots are color coded according to the speed of the fly with black arrows and
827 red dots indicating the initial and final positions, respectively. (D) Head intact and (E)
828 headless animals. Red arrow indicates a brief speed increase due to reflexive leg twitch.
829 At least 18 animals were used for each condition.
830

# Figure 2

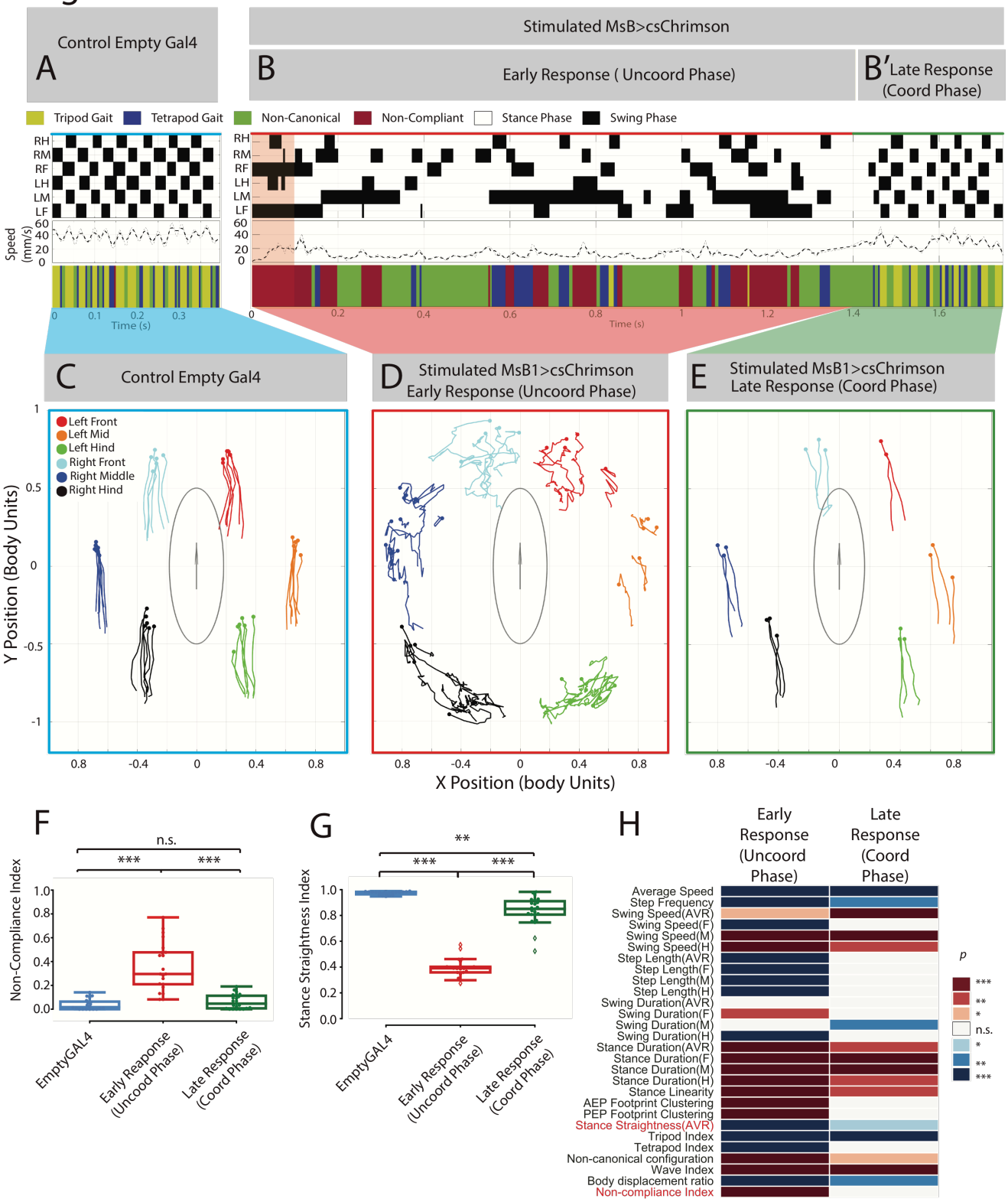
Control Empty Gal4
A
Stimulated MsB>csChrimson
B
Early Response ( Uncoord Phase)
B′ Late Response (Coord Phase)
Tripod Gait
Tetrapod Gait
Non-Canonical
Non-Compliant
Stance Phase
Swing Phase
RH
RM
RF
LH
LM
LF
Speed (mm/s)
Time (s)
C Control Empty Gal4
D Stimulated MsB1>csChrimson Early Response (Uncoord Phase)
E Stimulated MsB1>csChrimson Late Response (Coord Phase)
Left Front
Left Mid
Left Hind
Right Front
Right Middle
Right Hind
Y Position (Body Units)
X Position (body Units)
F
n.s.
***
Non-Compliance Index
EmptyGAL4
Early Reaponse (Uncood Phase)
Late Response (Coord Phase)
G
**
Stance Straightness Index
H
Early Response (Uncoord Phase)
Late Response (Coord Phase)
Average Speed
Step Frequency
Swing Speed(AVR)
Swing Speed(F)
Swing Speed(M)
Swing Speed(H)
Step Length(AVR)
Step Length(F)
Step Length(M)
Step Length(H)
Swing Duration(AVR)
Swing Duration(F)
Swing Duration(M)
Swing Duration(H)
Stance Duration(AVR)
Stance Duration(F)
Stance Duration(M)
Stance Duration(H)
Stance Linearity
AEP Footprint Clustering
PEP Footprint Clustering
Stance Straightness(AVR)
Tripod Index
Tetrapod Index
Non-canonical configuration
Wave Index
Body displacement ratio
Non-compliance Index
p
n.s.

832 **Figure 2. Kinematic analysis of walking patterns in MSB1 flies after**
833 **mechanosensory bristles stimulation**
834 (A-B) Representative gait features after MsB stimulation. Upper panel shows the flies'
835 step patterns across time. For each leg, swing phases are represented in black and stance
836 phases in white. Right hind (RH); right mid (RM); right front (RF); left hind (LH); left
837 middle (LM); left front (LF). Middle panel shows the instantaneous speed across time for
838 the same video. Thick and thin lines correspond to integration times of 25 or 12.5 ms,
839 respectively. Lower panel represents the gaits adopted by the fly during the period after
840 stimulation. For each frame the corresponding gait was color-coded as follows: Yellow
841 (tripod), blue (tetrapod), green (non-canonical), red (non-compliant configuration). See
842 Methods. (A) Empty GAL4 control (Genotype: empty-GAL44, $dac^{RE}$-flp, UAS-FRT-
843 stop-FRT-Chrimson-mVenus). (B) Post-stimulus response of MSB1 flies (Genotype:
844 R65D12-GAL4, $dac^{RE}$-flp, UAS-FRT-stop-FRT-Chrimson-mVenus). 100ms optogenetic
845 stimulation is represented by a red shadow. Sequence is divided in early response
846 (Uncoordinated Phase) and late response (Coordinated Phase) (B and B', respectively).
847 (C-E) Representative *stance traces*. Traces are generated by the position of the stance
848 phase footprints relative to the body center (set at 0.0,0.0). For each leg, stance onset
849 corresponds to the *Anterior Extreme Position* (*AEP*) (colored circle) while stance offset is
850 termed *Posterior Extreme Position* (*PEP*). Experimental conditions are color matched
851 with panels (A-B). (C) Control Empty GAL4 control. (D) Post-stimulus of MSB1 flies,
852 early response corresponding to the uncoordinated phase. (E) Post-stimulus of MSB1
853 flies, late response corresponding to the coordinated phase. (F-H) Kinematic
854 quantification between the empty GAL4 control and the early and late response post
855 stimulated (n=20 for each condition). In (F-G) boxplots represent the median as the
856 middle line, with the lower and upper edges of the boxes representing the 25% and 75%
857 quartiles, respectively, whiskers represent the range of the full data set, excluding outliers
858 represented by diamonds. Filled dots represent individual flies. Values are normalized for
859 body size. Statistical analysis with Kruskal–Wallis-ANOVA followed by Dunn's *post*
860 *hoc* analysis, **$p<0.01$, ***$p<0.001$. (F) *Non-Compliance Index* (G) *Stance straightness*
861 *index*. (H) Heat map of kinematic parameters comparing empty GAL4 control with early
862 response/ Uncoordinated Phase (first Column) and late response/Coordinated Phase

(second Column) of experimental group, with each line representing a motor parameter. Data were residual normalized and outliers were excluded. Statistical analysis with one-way ANOVA followed by Tukey's post hoc test (for normal distributions) or Kruskal–Wallis-ANOVA followed by Dunn's post hoc test (for non-normal distribution). p values are represented by a color code with red and blue shades indicate an increase or decrease or relative to control, respectively. *P<0.05; **P<0.01; ***P<0.001. White indicates no statistically significant variation.

# Figure 3

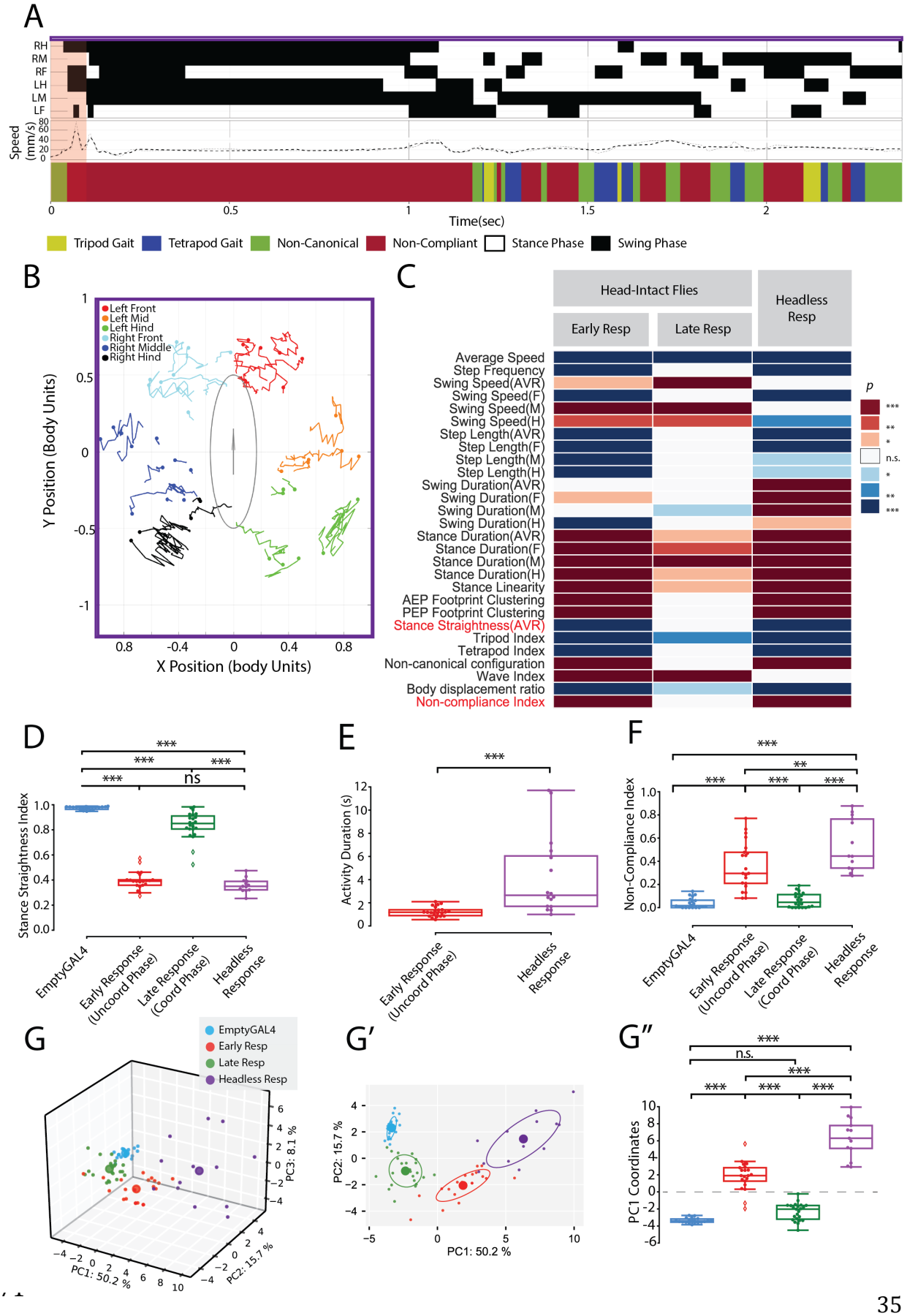
A
RH
RM
RF
LH
LM
LF
Speed (mm/s)
Time(sec)
Tripod Gait
Tetrapod Gait
Non-Canonical
Non-Compliant
Stance Phase
Swing Phase
B
Left Front
Left Mid
Left Hind
Right Front
Right Middle
Right Hind
Y Position (Body Units)
X Position (body Units)
C
Head-Intact Flies
Headless Resp
Early Resp
Late Resp
Average Speed
Step Frequency
Swing Speed(AVR)
Swing Speed(F)
Swing Speed(M)
Swing Speed(H)
Step Length(AVR)
Step Length(F)
Step Length(M)
Step Length(H)
Swing Duration(AVR)
Swing Duration(F)
Swing Duration(M)
Swing Duration(H)
Stance Duration(AVR)
Stance Duration(F)
Stance Duration(M)
Stance Duration(H)
Stance Linearity
AEP Footprint Clustering
PEP Footprint Clustering
Stance Straightness(AVR)
Tripod Index
Tetrapod Index
Non-canonical configuration
Wave Index
Body displacement ratio
Non-compliance Index
p
n.s.
D
Stance Straightness Index
EmptyGAL4
Early Response (Uncoord Phase)
Late Response (Coord Phase)
Headless Response
ns
E
Activity Duration (s)
Early Response (Uncoord Phase)
Headless Response
F
Non-Compliance Index
EmptyGAL4
Early Response (Uncoord Phase)
Late Response (Coord Phase)
Headless Response
G
EmptyGAL4
Early Resp
Late Resp
Headless Resp
PC1: 50.2 %
PC2: 15.7 %
PC3: 8.1 %
G′
PC2: 15.7 %
PC1: 50.2 %
G″
PC1 Coordinates
n.s.

872 **Figure 3. Mechanosensory Bristles evoked movement is independent of the central**
873 **Brain.**
874 (A) Representative gait features after MsB stimulation of headless flies. Genotype:
875 R65D12-GAL4, dac$^{RE}$-flp, UAS-FRT-stop-FRT-Chrimson-mVenus. Upper panel shows
876 the flies' step patterns across time. For each leg swing phases are represented in black
877 and stance phases in white. Right hind (RH); right mid (RM); right front (RF); left hind
878 (LH); left middle (LM); left front (LF). Middle panel shows the instantaneous speed
879 across time for the same video. Thick and thin lines correspond to integration times of 25
880 or 12.5 ms, respectively. Lower panel represents the gaits adopted by the fly during the
881 period after stimulation. For each frame the corresponding gait was color-coded as
882 follows: Yellow (tripod), blue (tetrapod), green (non-canonical), red (non-compliant
883 configurations). 100ms optogenetic stimulation is represented by a red shadow.
884 (B) Representative *stance traces* following optogenetic stimulation. Traces are generated
885 by the position of the stance phase footprints relative to the body center (set at 0.0,0.0).
886 For each leg, stance onset corresponds to the *Anterior Extreme Position* (*AEP*) (colored
887 circle) while stance offset is termed *Posterior Extreme Position* (*PEP*).
888 (C) Heat map of kinematic parameters comparing empty GAL4 control of head-intact
889 animals with the early/uncoordinated and late/coordinated responses (first and second
890 columns, respectively) of post-stimulated head-intact animals, and post-stimulated
891 headless flies (third column). Statistical analysis with one-way ANOVA followed by
892 Tukey's post hoc test (for normal distributions) or Kruskal–Wallis-ANOVA followed by
893 Dunn's post hoc test (for non-normal distribution). p values are represented by a color
894 code with red and blue shades indicate a decrease or increase relative to control,
895 respectively. *P<0.05; **P<0.01; ***P<0.001. White indicates no variation. (D) Stance
896 straightness index in head-intact empty GAL4 controls, early and late response of post-
897 stimulated head-intact animals, and post-stimulated headless flies. (E) Post stimulation
898 activity between head-intact (early response) and headless flies. (F) Non-Compliance
899 Index in head-intact empty GAL4 controls, early and late response of post-stimulated
900 head-intact animals, and post-stimulated headless flies. (G-G'') PCA of all kinematic
901 parameters in head-intact empty GAL4 controls, early and late response of post-
902 stimulated head-intact animals, and post-stimulated headless flies. (G) Tridimensional

representation of three-component PCA analysis. Each individual small dot represents one video while larger dots represent the average point (n=20 for each condition). Contribution of each component is indicated in each axis. (G') 2D representation of PC1-PC2 with ellipses delimiting 50% of variance of the data. (G'') Comparison of each PC1 coordinates. In (D-F, G'') boxplots represent the median as the middle line, with the lower and upper edges of the boxes representing the 25% and 75% quartiles, respectively, whiskers represent the range of the full data set, excluding outliers represented by diamonds. Filled dots represent individual flies. Values are normalized for body size. Statistical analysis with Kruskal–Wallis-ANOVA followed by Dunn's *post hoc* analysis, *$P < 0.05$; **$P < 0.01$; ***$P < 0.001$. (D) PC1 coordinates. (E) PC1 coordinates. See Methods for details.

Figure 4

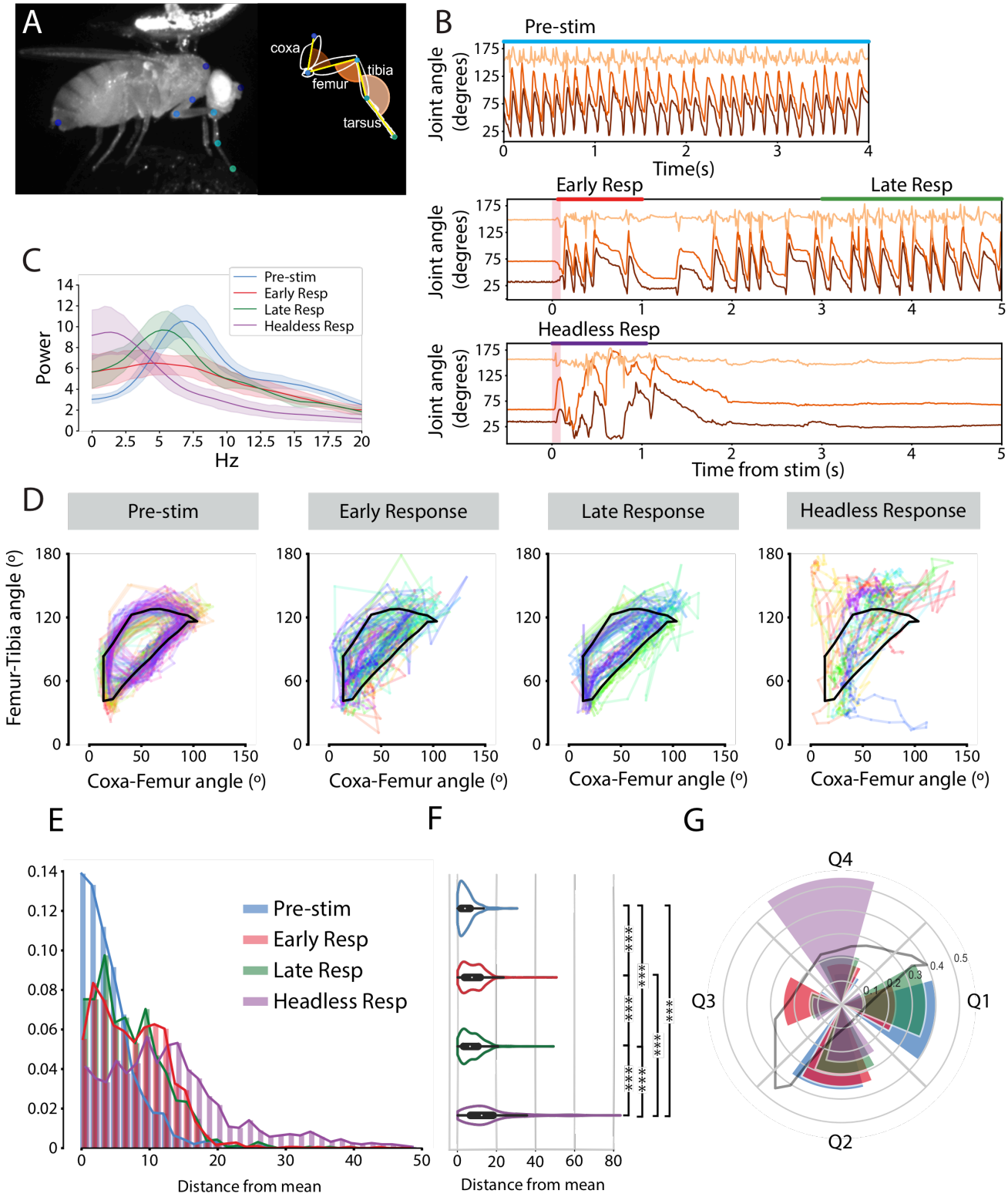
A
coxa
femur
tibia
tarsus
B
Pre-stim
Joint angle (degrees)
Time(s)
Early Resp
Late Resp
Headless Resp
Time from stim (s)
C
Pre-stim
Early Resp
Late Resp
Healdess Resp
Power
Hz
D
Pre-stim
Early Response
Late Response
Headless Response
Femur-Tibia angle (°)
Coxa-Femur angle (°)
E
Pre-stim
Early Resp
Late Resp
Headless Resp
Distance from mean
F
Distance from mean
G
Q1
Q2
Q3
Q4

915

**Figure 4. Mechanosensory Bristles evoked movement shows partially disrupted inter-joint coordination.**

(A) Tethered fly set-up showing tracked joint positions (blue/green circles). *Inset* schematic of Fly T1 leg showing 5 segments and 3 measured joint angles (Brown - Coxa-Femur angle, Bright Orange – Femur-Tibia angle, Light Orange – Tibia-Tarsus angle). B) Modulation of joint angles throughout time for our 4 experimental conditions: Walking flies (blue horizontal bar), Head-Intact Early Response (red horizontal bar), Head-Intact Late Response (green horizontal bar) and Headless Early Response (purple horizontal bar). Red transparent vertical bars in the mid and lower panel indicate the time of optogenetic stimulation. C) Fast Fourier Transform of leg angles for the Coxa-Femur Joint. D) Angle-angle plots of Coxa-Femur vs Femur-Tibia angles over time. Different colors represent individual trials. Black line indicates the mean trace of the 'walking' condition over the step cycle. E) Histogram of distances of points to the mean walking trace. (F) Violin plots for distances to mean walking trace. P values calculated using Dunns post-hoc test. ***$P < 0.001$ G) Frequency of occupancy for quadrants of the Coxa-Femur angle vs Femur-Tibia angle space.

# Figure 5

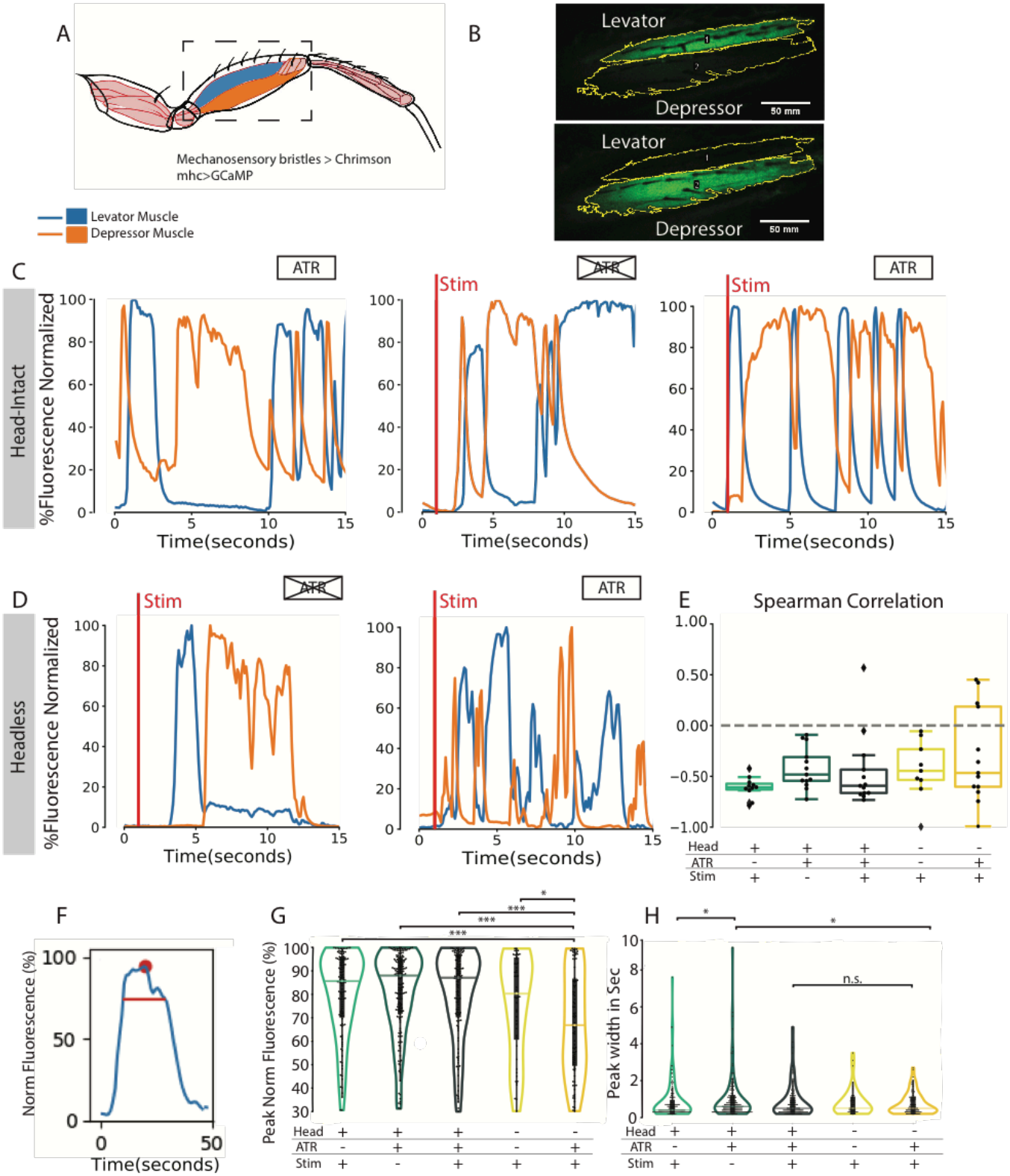
A
Mechanosensory bristles > Chrimson
mhc>GCaMP
Levator Muscle
Depressor Muscle
B
Levator
Depressor
50 mm
C
Head-Intact
%Fluorescence Normalized
ATR
Stim
Time(seconds)
D
Headless
E
Spearman Correlation
Head
ATR
Stim
F
Norm Fluorescence (%)
Time(seconds)
G
Peak Norm Fluorescence (%)
H
Peak width in Sec
n.s.

933

934 **Figure 5. Muscle activity alternation is maintained during sensory-triggered**
935 **movement**
936 (A) Leg schematic showing tibia levator (blue) and depressor (orange) muscles in the
937 femur. Adapted from (Venkatasubramanian et al., 2019). Dashed rectangle represents
938 scanned region of the genotype: lexO-GCaMP6f; mhc-lexA:LHV2, dacRE-flp;Uas-FRT-
939 stop-FRT-CsChrimson-mVenus, R65D12-Gal4 (B) Representative images of a femur
940 showing levator (top panel) or depressor muscle (lower panel) contraction, resulting in
941 GCaMP fluorescence inside the respective muscles. Yellow lines depict the ROIs used
942 for fluorescence calculations. (C-D) Representative plots showing the fluctuation of
943 fluorescence for levator (blue) and depressor (orange) muscle across time. Red bar
944 represents the 100 ms red light stimulation. Values are normalized to maximum signal
945 measured in each ROI throughout the experiment, corresponding to 100%. (C) Head-
946 intact animals. Left panel: Non-stimulated animals in the presence of All-Trans Retinal
947 (ATR), N=11; Middle Panel: Stimulated animals in the absence of ATR, N=13; Right
948 Panel: Stimulated animals in the presence of ATR. N=13 (D) Headless animals. Left
949 panel: Stimulated animals in the absence of ATR, N=12; Right Panel: Stimulated animals
950 in the presence of ATR, N=13. (E) Spearman correlation between levator and depressor
951 muscle activity for each experimental condition. Positive values indicate that muscles are
952 in-phase, while Negative values correspond to out of phase (antagonistic) activity.
953 Boxplots represent the median as the middle line, with the lower and upper edges of the
954 boxes representing the 25% and 75% quartiles, respectively, whiskers represent the range
955 of the full data set, excluding outliers represented by diamonds. Filled dots represent
956 individual flies. Statistical analysis with Kruskal–Wallis-ANOVA followed by Dunn's
957 *post hoc* analysis, no significant difference between the groups was detected (F)
958 Schematic showing muscle contraction curve analysis shown in (G) and (H). Red dot
959 indicates the maximum fluorescence value for the peak. Red line indicates the peak width
960 at 20% below peak level. (G) Violin plot showing the maximum value of fluorescence for
961 each contraction peak for each experimental condition. Each dot corresponds to a single
962 muscle contraction peak. Horizontal line represents the median. (H) Violin plot showing
963 the peak width for each contraction peak and each experimental condition. Each dot
964 corresponds to the width of a single muscle contraction peak. Horizontal line represents

965 the median. P values in (G, H) were calculated using Dunns post-hoc test. *P < 0.05; **P
966 < 0.01; ***P < 0.001
967

# Figure 6

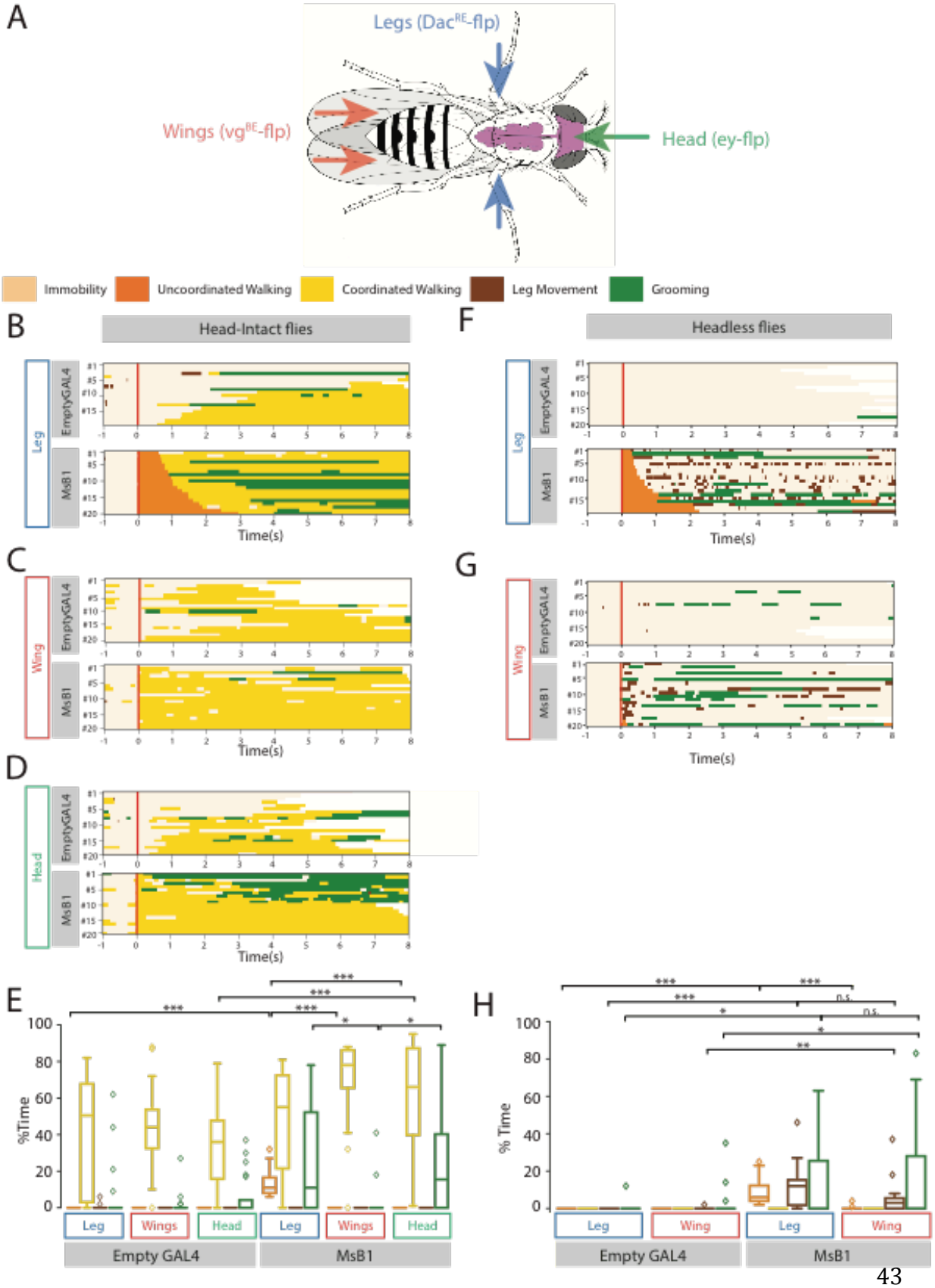
A
Legs (Dac^RE-flp)
Wings (vg^BE-flp)
Head (ey-flp)
Immobility
Uncoordinated Walking
Coordinated Walking
Leg Movement
Grooming
B
Head-Intact flies
F
Headless flies
C
G
D
Leg
Wing
Head
EmptyGAL4
MsB1
Time(s)
E
H
%Time
% Time
Leg
Wings
Head
Wing
Empty GAL4
MsB1
n.s.

969 **Figure 6. Cyclic movement is specific to leg MS bristle stimulation**
970 (A) Schematic showing the combinatorial genetic tools used to restrict the expression of
971 the MsB GAL4 driver R65D12 to the legs ($DAC^{RE}$-flp), wings ($Vg^{BE}$-flp) and head (ey-
972 flp) regions. Each combination was crossed with UAS>>CsChrimson. (B-D, F-G) Raster
973 plot showing the type of movement performed by the flies before and after the
974 stimulation of leg MsB. X axis represents the time in seconds where 0 is the moment of
975 the red light pulse stimulation (red Bar). Each line corresponds to one individual.
976 Movement categories: Immobility (beige); Uncoordinated walking (orange); Coordinated
977 walking (yellow); Leg movement (brown); and Grooming (green). Upper Panels shows
978 Empty GAL4 behavior while lower panel shows MSB1 GAL4 (R65D12) behavior (B-D)
979 Head-intact animals. (B) Leg domain (with $DAC^{RE}$-flp). (C) Wing domain (with $Vg^{BE}$-
980 flp). (D) Head domain (with ey-flp). (E, H) Percentage of time spent doing one of the
981 behaviors described for (B-D,F-G). Boxplots represent the median as the middle line,
982 with the lower and upper edges of the boxes representing the 25% and 75% quartiles,
983 respectively, whiskers represent the range of the full data set, excluding outliers
984 represented by diamonds. Statistical analysis with Kruskal–Wallis-ANOVA followed by
985 Dunn's *post hoc* analysis, *$p<0.05$ **$p<0.01$, ***$p<0.001$. (E) Quantification for head-
986 intact animals as shown in (B-D). (F-G) Headless flies. (F) Leg domain (with $DAC^{RE}$-
987 flp). (G) Wing domain (with $Vg^{BE}$-flp). (H) Quantification for head-intact animals as
988 shown in (F-G).
989

Figure 7

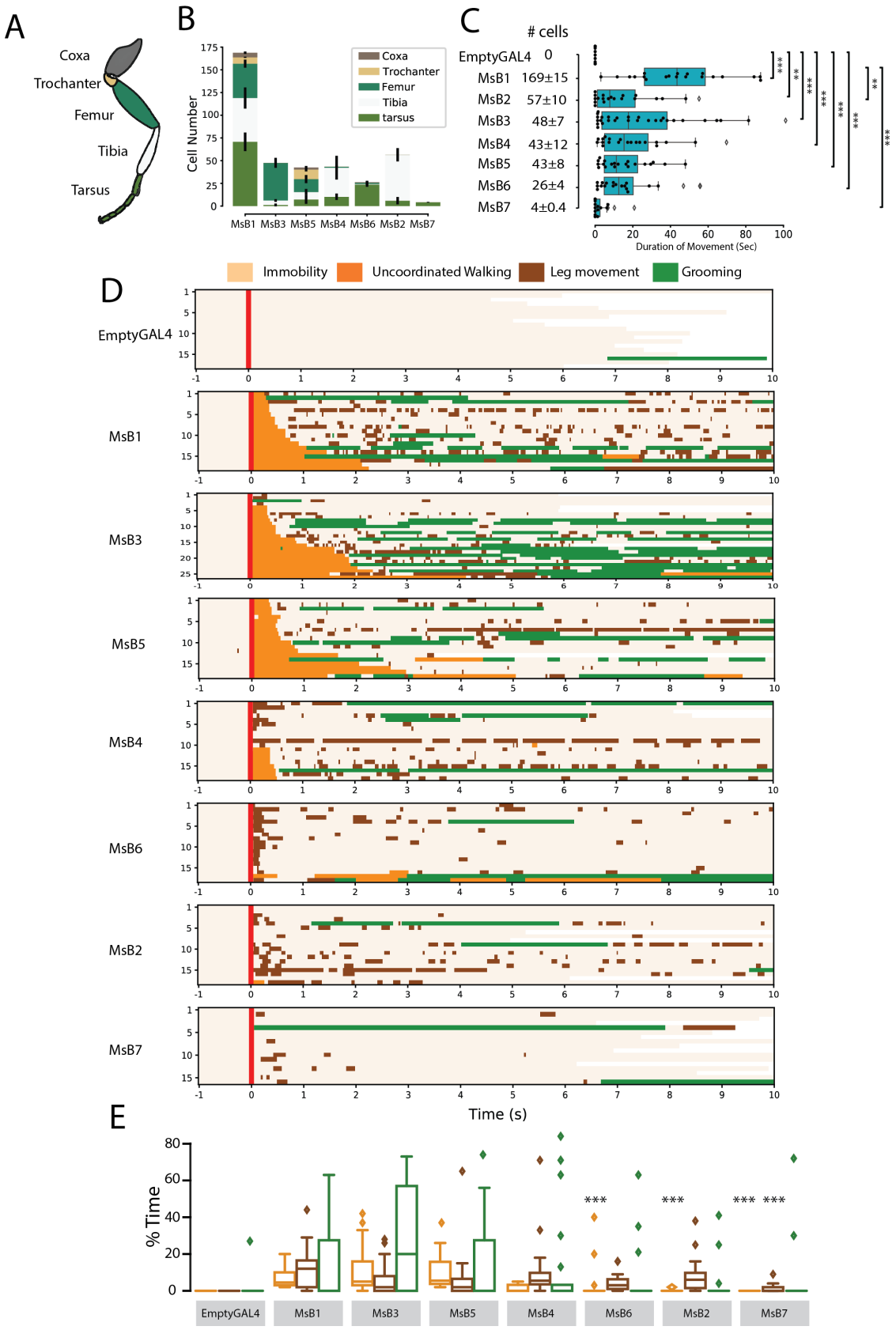
A
Coxa
Trochanter
Femur
Tibia
Tarsus
B
Cell Number
Coxa
Trochanter
Femur
Tibia
tarsus
MsB1 MsB3 MsB5 MsB4 MsB6 MsB2 MsB7
C
# cells
EmptyGAL4 0
MsB1 169±15
MsB2 57±10
MsB3 48±7
MsB4 43±12
MsB5 43±8
MsB6 26±4
MsB7 4±0.4
Duration of Movement (Sec)
D
Immobility
Uncoordinated Walking
Leg movement
Grooming
EmptyGAL4
MsB1
MsB3
MsB5
MsB4
MsB6
MsB2
MsB7
Time (s)
E
% Time
EmptyGAL4
MsB1
MsB3
MsB5
MsB4
MsB6
MsB2
MsB7

990

991 **Figure 7. Movement pattern triggered by distinct leg MsB populations in headless**
992 **animals**
993 (A) Schematic depicting the leg segments of the of *Drosophila melanogaster*. (B) Cell
994 labelling distribution amongst leg segments for each line. Error bar represent standard
995 deviation. MSB1: R65D12[leg], MSB2:R77E09[leg], MSB3:R39A11[leg], MSB4:
996 R54A11[leg], MSB5: R64D07[leg], MSB6: R85A07[leg], MSB7: R45D07[leg]. (C)
997 Duration of movement after one pulse of red light stimulation (100ms) for each MSB
998 line. Lines are organized according to the number of labeled cells in an ascending order.
999 (D) Raster plots showing the type of movement performed by the flies in each group, 1
1000 second before and up to 10 seconds after the stimulation. X axis represent the time in
1001 seconds being 0 the time of optogenetic stimulation (red Bar). Each line corresponds to
1002 one individual. The categorization of movements includes Immobility (beige),
1003 Uncoordinated Walking (orange), Leg Displacement (brown); and Grooming (green).
1004 Lines are ordered in descending order according to the length of uncoordinated walking
1005 response (E) Boxplots showing for each MSB line the percentage of time spent doing a
1006 specific behavior. Behaviors are color-coded as in panel D. Boxplots represent the
1007 median as the middle line, with the lower and upper edges of the boxes representing the
1008 25% and 75% quartiles, respectively, whiskers represent the range of the full data set,
1009 excluding outliers represented by diamonds. Statistical analysis with Kruskal–Wallis-
1010 ANOVA followed by Dunn's *post hoc* analysis, *$p<0.05$, **$p<0.01$, ***$p<0.001$.
1011

1012 **Lead Contact and Material Availability**

1013 Further information and requests for resources and reagents should be directed to and will
1014 be fulfilled by the Lead Contact, César S. Mendes (cesar.mendes@nms.unl.pt). The fly
1015 lines generated in this study are available from the Lead Contact without restrictions.

1016

1017

1018

1019 **Acknowledgements**

1020

1021 We thank Mendes lab, Rita Teodoro and her lab for comments and suggestions during the
1022 execution of this project, Allan Mancoo for feedback on data analysis, Inês Fernandes for
1023 experimental assistance, and Luísa Vasconcelos, Turgay Akay and Daniela Pereira for
1024 comments on the manuscript. We thank Mirian Zecca and Richard Mann for support
1025 generating the transgenic lines used in this study. We also thank CONGENTO:
1026 consortium for genetically tractable organisms, the Fly Platform and the Scientific
1027 Hardware Platform at the Champalimaud Centre for the Unknown, and the Bloomington
1028 Drosophila Stock Center for fly stocks. This work was supported by Fundação para a
1029 Ciência e a Tecnologia (FCT) (PTDC/BIA-COM/0151/2020), iNOVA4Health
1030 (UIDB/04462/2020 and UIDP/04462/2020), and LS4FUTURE (LA/P/0087/2020) to
1031 CSM. AM was supported by a doctoral fellowship from FCT (PD/BD/128445/2017).

1032

1033 **Author contributions**

1034

1035 AMM, AFH and CM contributed to conception and design of the study. AMM performed
1036 the experiments and analyzed the raw data; AFH performed data acquisition and analysis
1037 of Figure 4, and contributed to the analysis of Figure 5 data. GB contributed for analysis
1038 and data acquisition of Figure 7. AMM, AFH, MM and CSM wrote the manuscript. All
1039 authors contributed to manuscript revision, read, and approved the submitted version.

1040

1041 **Declaration of interests**

1042

The authors declare no competing interests.

## References


Agrawal, S., Dickinson, E.S., Sustar, A., Gurung, P., Shepherd, D., Truman, J.W., and Tuthill, J.C. (2020). Central processing of leg proprioception in Drosophila. Elife *9*.

Akay, T., Bässler, U., Gerharz, P., and Büschges, A. (2001). The role of sensory signals from the insect coxa-trochanteral joint in controlling motor activity of the femur-tibia joint. Journal of neurophysiology *85*, 594-604.

Akay, T., and Büschges, A. (2006). Load signals assist the generation of movement-dependent reflex reversal in the femur-tibia joint of stick insects. Journal of neurophysiology *96*, 3532-3537.

Akay, T., Ludwar, B., Goritz, M.L., Schmitz, J., and Buschges, A. (2007). Segment specificity of load signal processing depends on walking direction in the stick insect leg muscle control system. J Neurosci *27*, 3285-3294.

Akay, T., Tourtellotte, W.G., Arber, S., and Jessell, T.M. (2014). Degradation of mouse locomotor pattern in the absence of proprioceptive sensory feedback. Proc Natl Acad Sci U S A *111*, 16877-16882.

Alexander, R.M. (2003). Principles of Animal Locomotion, STU - Student edition edn (Princeton University Press).

Angeli, C.A., Edgerton, V.R., Gerasimenko, Y.P., and Harkema, S.J. (2014). Altering spinal cord excitability enables voluntary movements after chronic complete paralysis in humans. Brain *137*, 1394-1409.

Ballermann, M., and Fouad, K. (2006). Spontaneous locomotor recovery in spinal cord injured rats is accompanied by anatomical plasticity of reticulospinal fibers. Eur J Neurosci *23*, 1988-1996.

Bareyre, F.M., Kerschensteiner, M., Raineteau, O., Mettenleiter, T.C., Weinmann, O., and Schwab, M.E. (2004). The injured spinal cord spontaneously forms a new intraspinal circuit in adult rats. Nat Neurosci *7*, 269-277.

Barrios, N., Farias, M., and Moita, M.A. (2021). Threat induces cardiac and metabolic changes that negatively impact survival in flies. Current biology : CB *31*, 5462-5472.e5464.

Bassler, U., and Buschges, A. (1998). Pattern generation for stick insect walking movements--multisensory control of a locomotor program. Brain Res Brain Res Rev *27*, 65-88.

Baudoux, S., Duch, C., and Morris, O.T. (1998). Coupling of efferent neuromodulatory neurons to rhythmical leg motor activity in the locust. J Neurophysiol *79*, 361-370.

1080 Bidaye, S.S., Bockemühl, T., and Büschges, A. (2018). Six-legged walking in insects: how
1081 CPGs, peripheral feedback, and descending signals generate coordinated and
1082 adaptive motor rhythms. Journal of neurophysiology *119*, 459-475.

1083 Borgmann, A., Toth, T.I., Gruhn, M., Daun-Gruhn, S., and Büschges, A. (2011).
1084 Dominance of local sensory signals over inter-segmental effects in a motor system:
1085 experiments. Biol Cybern *105*, 399-411.

1086 Brown, T.G. (1911 ). The intrinsic factors in the act of progression in the mammal.
1087 Proceedings of the Royal Society of London Series B, containing papers of a
1088 biological character *84*, 308-319.

1089 Buchner, E. (1976). Elementary movement detectors in an insect visual system.
1090 Biological Cybernetics *24*, 85-101.

1091 Burrows, M. (1996). The Neurobiology of an Insect Brain (Oxford University Press).

1092 Burrows, M., Laurent, G.J., and Field, L.H. (1988). Proprioceptive inputs to nonspiking
1093 local interneurons contribute to local reflexes of a locust hindleg. J Neurosci *8*, 3085-
1094 3093.

1095 Buschges, A. (1995). Role of local nonspiking interneurons in the generation of
1096 rhythmic motor activity in the stick insect. J Neurobiol *27*, 488-512.

1097 Büschges, A., Schmitz, J., and Bässler, U. (1995). Rhythmic patterns in the thoracic
1098 nerve cord of the stick insect induced by pilocarpine. Journal of Experimental
1099 Biology *198*, 435-456.

1100 Cabrita, A., Medeiros, A.M., Pereira, T., Rodrigues, A.S., Kranendonk, M., and Mendes,
1101 C.S. (2022). Motor dysfunction in Drosophila melanogaster as a biomarker for
1102 developmental neurotoxicity. iScience *25*, 104541.

1103 Cande, J., Namiki, S., Qiu, J., Korff, W., Card, G.M., Shaevitz, J.W., Stern, D.L., and Berman,
1104 G.J. (2018). Optogenetic dissection of descending behavioral control in Drosophila.
1105 eLife *7*, e34275.

1106 Capogrosso, M., Wenger, N., Raspopovic, S., Musienko, P., Beauparlant, J., Bassi Luciani,
1107 L., Courtine, G., and Micera, S. (2013). A computational model for epidural electrical
1108 stimulation of spinal sensorimotor circuits. J Neurosci *33*, 19326-19340.

1109 Chen, C., Agrawal, S., Mark, B., Mamiya, A., Sustar, A., Phelps, J.S., Lee, W.-C.A., Dickson,
1110 B.J., Card, G.M., and Tuthill, J.C. (2021). Functional architecture of neural circuits for
1111 leg proprioception in Drosophila. Current Biology *31*, 5163-5175.e5167.

1112 Cheng, L.E., Song, W., Looger, L.L., Jan, L.Y., and Jan, Y.N. (2010). The role of the TRP
1113 channel NompC in Drosophila larval and adult locomotion. Neuron *67*, 373-380.

1114 Chrachri, A., and Clarac, F. (1987). Induction of rhythmic activity in motoneurons of
1115 crayfish thoracic ganglia by cholinergic agonists. Neurosci Lett *77*, 49-54.

1116 Court, R., Namiki, S., Armstrong, J.D., Börner, J., Card, G., Costa, M., Dickinson, M., Duch,
1117 C., Korff, W., Mann, R.*, et al.* (2020). A Systematic Nomenclature for the Drosophila
1118 Ventral Nerve Cord. Neuron *107*, 1071-1079.e1072. doi:
1119 1010.1016/j.neuron.2020.1008.1005. Epub 2020 Sep 1014.

1120 Courtine, G., Song, B., Roy, R.R., Zhong, H., Herrmann, J.E., Ao, Y., Qi, J., Edgerton, V.R.,
1121 and Sofroniew, M.V. (2008). Recovery of supraspinal control of stepping via indirect
1122 propriospinal relay connections after spinal cord injury. Nat Med *14*, 69-74.

1123 Cruse, H., and Bartling, C. (1995). Movement of Joint Angles in the Legs of a Walking
1124 Insect, Carausius morosus. J Insecr Physiol *41*, 761-771.

1125 Daun, S., Mantziaris, C., Tóth, T., Büschges, A., and Rosjat, N. (2019). Unravelling intra-
1126 and intersegmental neuronal connectivity between central pattern generating
1127 networks in a multi-legged locomotor system. PLoS One *14*, e0220767.

1128 David, I., Holmes, P., and Ayali, A. (2016). Endogenous rhythm and pattern-generating
1129 circuit interactions in cockroach motor centres. Biol Open *5*, 1229-1240.

1130 DeAngelis, B.D., Zavatone-Veth, J.A., Gonzalez-Suarez, A.D., and Clark, D.A. (2020).
1131 Spatiotemporally precise optogenetic activation of sensory neurons in freely
1132 walking Drosophila. eLife *9*, e54183.

1133 Dickinson, M.H., Farley, C.T., Full, R.J., Koehl, M.A., Kram, R., and Lehman, S. (2000). How
1134 animals move: an integrative view. Science *288*, 100-106.

1135 Durr, V., Schmitz, J., and Cruse, H. (2004). Behaviour-based modelling of hexapod
1136 locomotion: linking biology and technical application. Arthropod Struct Dev *33*, 237-
1137 250.

1138 Eccles, J.C., Fatt, P., and Landgren, S. (1956). Central pathway for direct inhibitory
1139 action of impulses in largest afferent nerve fibres to muscle. J Neurophysiol *19*, 75-
1140 98.

1141 Feng, K., Sen, R., Minegishi, R., Dubbert, M., Bockemuhl, T., Buschges, A., and Dickson,
1142 B.J. (2020). Distributed control of motor circuits for backward walking in
1143 Drosophila. Nat Commun *11*, 6166.

1144 Formento, E., Minassian, K., Wagner, F., Mignardot, J.B., Le Goff-Mignardot, C.G., Rowald,
1145 A., Bloch, J., Micera, S., Capogrosso, M., and Courtine, G. (2018). Electrical spinal cord
1146 stimulation must preserve proprioception to enable locomotion in humans with
1147 spinal cord injury. Nat Neurosci *21*, 1728-1741.

1148 Fuchs, E., Holmes, P., Kiemel, T., and Ayali, A. (2011). Intersegmental coordination of
1149 cockroach locomotion: adaptive control of centrally coupled pattern generator
1150 circuits. Front Neural Circuits *4*, 125.

1151 Gao, Q., Yuan, B., and Chess, A. (2000). Convergent projections of Drosophila olfactory
1152 neurons to specific glomeruli in the antennal lobe. Nat Neurosci *3*, 780-785.

1153 Goldammer, J., Mantziaris, C., Büschges, A., and Schmidt, J. (2018). Calcium imaging of
1154 CPG-evoked activity in efferent neurons of the stick insect. PLoS One *13*, e0202822.

1155 Götz, K.G., and Wenking, H. (1973). Visual control of locomotion in the walking
1156 fruitflyDrosophila. Journal of comparative physiology *85*, 235-266.

1157 Grillner, S. (1975). Locomotion in vertebrates: central mechanisms and reflex
1158 interaction. Physiol Rev *55*, 247-304.

1159 Hampel, S., McKellar, C.E., Simpson, J.H., and Seeds, A.M. (2017). Simultaneous
1160 activation of parallel sensory pathways promotes a grooming sequence in
1161 Drosophila. Elife *6*.

1162 Heredia, F., Volonté, Y., Pereirinha, J., Fernandez-Acosta, M., Casimiro, A.P., Belém, C.G.,
1163 Viegas, F., Tanaka, K., Menezes, J., Arana, M.*, et al.* (2021). The steroid-hormone
1164 ecdysone coordinates parallel pupariation neuromotor and morphogenetic
1165 subprograms via epidermis-to-neuron Dilp8-Lgr3 signal induction. Nat Commun *12*,
1166 3328.

1167 Hoyt, D.F., and Taylor, R. (1981). Gait and the energetics of locomotion in horses.
1168 Nature *292*, 239-240.

1169 Jarman, A.P., Grau, Y., Jan, L.Y., and Jan, Y.N. (1993). atonal is a proneural gene that
1170 directs chordotonal organ formation in the Drosophila peripheral nervous system.
1171 Cell *73*, 1307-1321.

1172 Jenett, A., Rubin, G.M., Ngo, T.T., Shepherd, D., Murphy, C., Dionne, H., Pfeiffer, B.D.,
1173 Cavallaro, A., Hall, D., Jeter, J.*, et al.* (2012). A GAL4-driver line resource for
1174 Drosophila neurobiology. Cell Rep *2*, 991-1001.

1175 Juvin, L., Le Gal, J.-P., Simmers, J., and Morin, D. (2012). Cervicolumbar Coordination in
1176 Mammalian Quadrupedal Locomotion: Role of Spinal Thoracic Circuitry and Limb
1177 Sensory Inputs. The Journal of Neuroscience *32*, 953.

1178 Kain, P., and Dahanukar, A. (2015). Secondary taste neurons that convey sweet taste
1179 and starvation in the Drosophila brain. Neuron *85*, 819-832.

1180 Kamikouchi, A., Wiek, R., Effertz, T., Göpfert, M.C., and Fiala, A. (2010). Transcuticular
1181 optical imaging of stimulus-evoked neural activities in the Drosophila peripheral
1182 nervous system. Nat Protoc *5*, 1229-1235.

1183 King, D.G., and Wyman, R.J. (1980). Anatomy of the giant fibre pathway in Drosophila. I.
1184 Three thoracic components of the pathway. Journal of Neurocytology *9*, 753-770.

1185 Kittmann, R., and Schmitz, J. (1992). FUNCTIONAL SPECIALIZATION OF THE
1186 SCOLOPARIA OF THE FEMORAL CHORDOTONAL ORGAN IN STICK INSECTS. Journal
1187 of Experimental Biology *173*, 91-108.

1188 Li, J., Zhang, W., Guo, Z., Wu, S., Jan, L.Y., and Jan, Y.N. (2016). A Defensive Kicking
1189 Behavior in Response to Mechanical Stimuli Mediated by Drosophila Wing Margin
1190 Bristles. J Neurosci *36*, 11275-11282. doi: 11210.11523/JNEUROSCI.11416-
1191 11216.12016.

1192 Lopes, G., Bonacchi, N., Frazao, J., Neto, J.P., Atallah, B.V., Soares, S., Moreira, L., Matias,
1193 S., Itskov, P.M., Correia, P.A.*, et al.* (2015). Bonsai: an event-based framework for
1194 processing and controlling data streams. Front Neuroinform *9*, 7.

1195 Mamiya, A., Gurung, P., and Tuthill, J.C. (2018). Neural Coding of Leg Proprioception in
1196 Drosophila. Neuron *100*, 636-650.e636.

1197 Mantziaris, C., Bockemühl, T., Holmes, P., Borgmann, A., Daun, S., and Büschges, A.
1198 (2017). Intra- and intersegmental influences among central pattern generating

networks in the walking system of the stick insect. Journal of neurophysiology *118*, 2296-2310.

Mathis, A., Mamidanna, P., Cury, K.M., Abe, T., Murthy, V.N., Mathis, M.W., and Bethge, M. (2018). DeepLabCut: markerless pose estimation of user-defined body parts with deep learning. Nature neuroscience *21*, 1281-1289.

Meissner, G.W., Nern, A., Dorman, Z., DePasquale, G.M., Forster, K., Gibney, T., Hausenfluck, J.H., He, Y., Iyer, N., Jeter, J.*, et al.* (2022). A searchable image resource of <em>Drosophila</em> GAL4-driver expression patterns with single neuron resolution. bioRxiv, 2020.2005.2029.080473.

Mendes, C.S., Bartos, I., Akay, T., Marka, S., and Mann, R.S. (2013). Quantification of gait parameters in freely walking wild type and sensory deprived Drosophila melanogaster. Elife *2*, e00231.

Mendes, C.S., Rajendren, S.V., Bartos, I., Marka, S., and Mann, R.S. (2014). Kinematic responses to changes in walking orientation and gravitational load in Drosophila melanogaster. PLoS One *9*, e109204.

Merritt, D.J., and Murphey, R.K. (1992). Projections of leg proprioceptors within the CNS of the fly Phormia in relation to the generalized insect ganglion. J Comp Neurol *322*, 16-34.

Murphey, R.K., Possidente, D.R., Vandervorst, P., and Ghysen, A. (1989). Compartments and the topography of leg afferent projections in Drosophila. J Neurosci *9*, 3209-3217.

Namiki, S., Dickinson, M.H., Wong, A.M., Korff, W., and Card, G.M. (2018). The functional organization of descending sensory-motor pathways in Drosophila. eLife *7*, e34272.

Pearson, K.G. (1972). Central Programming and Reflex Control of Walking in the Cockroach. Journal of Experimental Biology *56*, 173-193.

Pearson, K.G., and Fourtner, C.R. (1975). Nonspiking interneurons in walking system of the cockroach. J Neurophysiol *38*, 33-52.

Pfeiffer, B.D., Ngo, T.T., Hibbard, K.L., Murphy, C., Jenett, A., Truman, J.W., and Rubin, G.M. (2010). Refinement of tools for targeted gene expression in Drosophila. Genetics *186*, 735-755.

Phelps, J.S., Hildebrand, D.G.C., Graham, B.J., Kuan, A.T., Thomas, L.A., Nguyen, T.M., Buhmann, J., Azevedo, A.W., Sustar, A., Agrawal, S.*, et al.* (2021). Reconstruction of motor control circuits in adult Drosophila using automated transmission electron microscopy. Cell *184*, 759-774.e718. doi: 710.1016/j.cell.2020.1012.1013. Epub 2021 Jan 1014.

Ramdya, P., Lichocki, P., Cruchet, S., Frisch, L., Tse, W., Floreano, D., and Benton, R. (2015). Mechanosensory interactions drive collective behaviour in Drosophila. Nature *519*, 233-236.

1237 Rillich, J., Stevenson, P.A., and Pflueger, H.J. (2013). Flight and walking in locusts-
1238 cholinergic co-activation, temporal coupling and its modulation by biogenic amines.
1239 PLoS One *8*, e62899.

1240 Ritzmann, R.E., and Buschges, A. (2007). Adaptive motor behavior in insects. Curr Opin
1241 Neurobiol *17*, 629-636.

1242 Rosenbaum, P., Wosnitza, A., Buschges, A., and Gruhn, M. (2010). Activity patterns and
1243 timing of muscle activity in the forward walking and backward walking stick insect
1244 Carausius morosus. Journal of neurophysiology *104*, 1681-1695.

1245 Ryckebusch, S., and Laurent, G. (1993). Rhythmic patterns evoked in locust leg motor
1246 neurons by the muscarinic agonist pilocarpine. J Neurophysiol *69*, 1583-1595.

1247 Ryckebusch, S., and Laurent, G. (1994). Interactions between segmental leg central
1248 pattern generators during fictive rhythms in the locust. J Neurophysiol *72*, 2771-
1249 2785.

1250 Seeds, A.M., Ravbar, P., Chung, P., Hampel, S., Midgley, F.M., Jr., Mensh, B.D., and
1251 Simpson, J.H. (2014). A suppression hierarchy among competing motor programs
1252 drives sequential grooming in Drosophila. Elife *3*, e02951.

1253 Seelig, J.D., Chiappe, M.E., Lott, G.K., Dutta, A., Osborne, J.E., Reiser, M.B., and Jayaraman,
1254 V. (2010). Two-photon calcium imaging from head-fixed Drosophila during
1255 optomotor walking behavior. Nature methods *7*, 535-540.

1256 Shanbhag, S.R., Singh, K., and Naresh Singh, R. (1992). Ultrastructure of the femoral
1257 chordotonal organs and their novel synaptic organization in the legs of Drosophila
1258 melanogaster Meigen (Diptera : Drosophilidae). International Journal of Insect
1259 Morphology and Embryology *21*, 311-322.

1260 Sherrington, C.S. (1893). Further Experimental Note on the Correlation of Action of
1261 Antagonistic Muscles. Br Med J *1*, 1218.

1262 Siegler, M.V., and Burrows, M. (1986). Receptive fields of motor neurons underlying
1263 local tactile reflexes in the locust. J Neurosci *6*, 507-513.

1264 Smith, S.A., and Shepherd, D. (1996). Central afferent projections of proprioceptive
1265 sensory neurons in Drosophila revealed with the enhancer-trap technique. J Comp
1266 Neurol *364*, 311-323.

1267 Soler, C., Daczewska, M., Da Ponte, J.P., Dastugue, B., and Jagla, K. (2004). Coordinated
1268 development of muscles and tendons of the Drosophila leg. Development *131*, 6041-
1269 6051.

1270 Strausfeld, N.J., Bassemir, U., Singh, R.N., and Bacon, J.P. (1984). Organizational
1271 principles of outputs from Dipteran brains. Journal of Insect Physiology *30*, 73-93.

1272 Strauss, R., and Heisenberg, M. (1990). Coordination of legs during straight walking
1273 and turning in Drosophila melanogaster. J Comp Physiol A *167*, 403-412.

1274 Szczecinski, N.S., Bockemuhl, T., Chockley, A.S., and Buschges, A. (2018). Static stability
1275 predicts the continuum of interleg coordination patterns in Drosophila. J Exp Biol
1276 *221*.

1277 Takeoka, A., Vollenweider, I., Courtine, G., and Arber, S. (2014). Muscle spindle
1278 feedback directs locomotor recovery and circuit reorganization after spinal cord
1279 injury. Cell *159*, 1626-1639.

1280 Tanouye, M.A., and Wyman, R.J. (1980). Motor outputs of giant nerve fiber in
1281 Drosophila. Journal of Neurophysiology *44*, 405-421.

1282 Trimarchi, J.R., and Schneiderman, A.M. (1995). Flight initiations in Drosophila
1283 melanogaster are mediated by several distinct motor patterns. Journal of
1284 Comparative Physiology A *176*, 355-364.

1285 Tsubouchi, A., Yano, T., Yokoyama, T.K., Murtin, C., Otsuna, H., and Ito, K. (2017).
1286 Topological and modality-specific representation of somatosensory information in
1287 the fly brain. Science *358*, 615-623.

1288 Tuthill, J.C., and Wilson, R.I. (2016a). Mechanosensation and Adaptive Motor Control in
1289 Insects. Curr Biol *26*, R1022-R1038.

1290 Tuthill, J.C., and Wilson, R.I. (2016b). Parallel Transformation of Tactile Signals in
1291 Central Circuits of Drosophila. Cell *164*, 1046-1059.

1292 Vandervorst, P., and Ghysen, A. (1980). Genetic control of sensory connections in
1293 Drosophila. Nature *286*, 65-67.

1294 Venkatasubramanian, L., Guo, Z., Xu, S., Tan, L., Xiao, Q., Nagarkar-Jaiswal, S., and Mann,
1295 R.S. (2019). Stereotyped terminal axon branching of leg motor neurons mediated by
1296 IgSF proteins DIP-α and Dpr10. eLife *8*, e42692.

1297 Wagner, F.B., Mignardot, J.B., Le Goff-Mignardot, C.G., Demesmaeker, R., Komi, S.,
1298 Capogrosso, M., Rowald, A., Seanez, I., Caban, M., Pirondini, E.*, et al.* (2018). Targeted
1299 neurotechnology restores walking in humans with spinal cord injury. Nature *563*,
1300 65-71.

1301 Williams, J.A., Paddock, S.W., Vorwerk, K., and Carroll, S.B. (1994). Organization of wing
1302 formation and induction of a wing-patterning gene at the dorsal/ventral
1303 compartment boundary. Nature *368*, 299-305.

1304 Wosnitza, A., Bockemuhl, T., Dubbert, M., Scholz, H., and Buschges, A. (2013). Inter-leg
1305 coordination in the control of walking speed in Drosophila. J Exp Biol *216*, 480-491.

1306 Wu, M., Nern, A., Williamson, W.R., Morimoto, M.M., Reiser, M.B., Card, G.M., and Rubin,
1307 G.M. (2016). Visual projection neurons in the Drosophila lobula link feature
1308 detection to distinct behavioral programs. Elife *5*.

1309 Yellman, C., Tao, H., He, B., and Hirsh, J. (1997). Conserved and sexually dimorphic
1310 behavioral responses to biogenic amines in decapitated Drosophila. Proc Natl Acad
1311 Sci U S A *94*, 4131-4136.

1312 Zecca, M., and Struhl, G. (2007). Control of Drosophila wing growth by the vestigial
1313 quadrant enhancer. Development (Cambridge, England) *134*, 3011-3020.

1314 zur Lage, P.I., Powell, L.M., Prentice, D.R., McLaughlin, P., and Jarman, A.P. (2004). EGF
1315 receptor signaling triggers recruitment of Drosophila sense organ precursors by
1316 stimulating proneural gene autoregulation. Dev Cell *7*, 687-696.

1317